Cell Reports

Acute SARS-CoV-2 infection is associated with an increased abundance of bacterial pathogens, including *Pseudomonas aeruginosa* in the nose

Graphical abstract

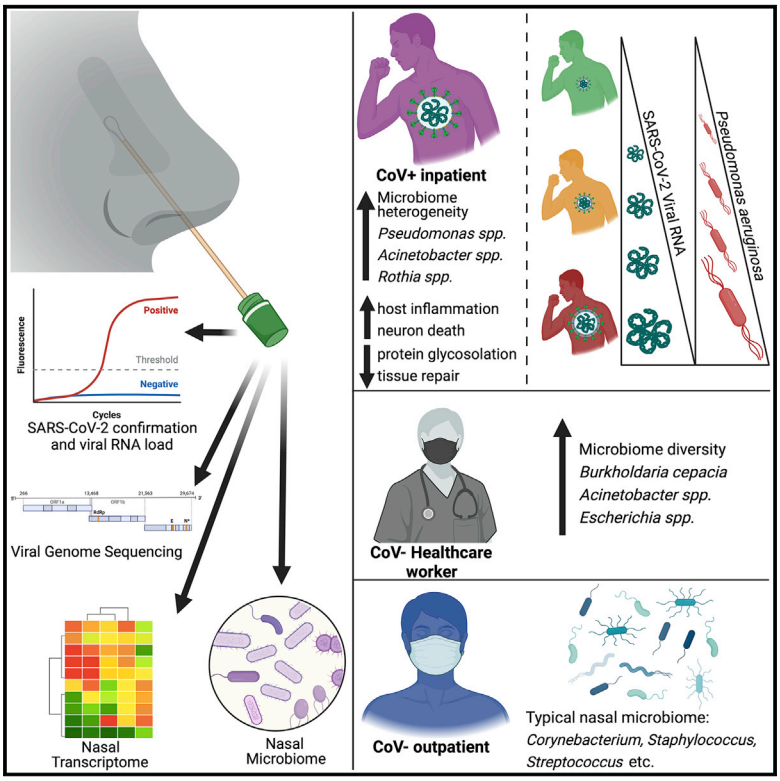

Highlights

- Acute SARS-CoV-2 infection is associated with shifts in the nasal microbiome
- Abundance of *Pseudomonas aeruginosa* increases with SARS-CoV-2 viral RNA load
- Healthcare providers and infected patients share some nasal microbiome features
- The nasal transcriptome of infected patients reveals inflammation and neuron damage

Authors

Nicholas S. Rhoades, Amanda N. Pinski, Alisha N. Monsibais, ..., Isaac R. Cinco, Izabela Ibraim, Ilhem Messaoudi

Correspondence

imessaou@uci.edu

In brief

Rhoades et al. show that patients acutely infected with SARS-CoV-2 have a distinct nasal microbiome marked by an increase in bacterial pathogens such as *Pseudomonas aeruginosa* and accompanied by a robust inflammatory host transcriptional response. This provides a potential explanation for the high rate of bacterial co-infections in COVID-19 patients.

Rhoades et al., 2021, Cell Reports *36*, 109637
August 31, 2021
https://doi.org/10.1016/j.celrep.2021.109637

CellPress

Cell Reports

CellPress
OPEN ACCESS

Report

Acute SARS-CoV-2 infection is associated with an increased abundance of bacterial pathogens, including *Pseudomonas aeruginosa* in the nose

Nicholas S. Rhoades,[1] Amanda N. Pinski,[1] Alisha N. Monsibais,[1] Allen Jankeel,[1] Brianna M. Doratt,[1] Isaac R. Cinco,[1] Izabela Ibraim,[1] and Ilhem Messaoudi[1,2,*]

[1]Department of Molecular Biology and Biochemistry, University of California Irvine, Irvine, CA, USA

[2]Lead contact

*Correspondence: imessaou@uci.edu

https://doi.org/10.1016/j.celrep.2021.109637

SUMMARY

Research conducted on severe acute respiratory syndrome coronavirus 2 (SARS-CoV-2) pathogenesis and coronavirus disease 2019 (COVID-19) generally focuses on the systemic host response, especially that generated by severely ill patients, with few studies investigating the impact of acute SARS-CoV-2 at the site of infection. We show that the nasal microbiome of SARS-CoV-2-positive patients (CoV^+, n = 68) at the time of diagnosis is unique when compared to CoV^- healthcare workers (n = 45) and CoV^- outpatients (n = 21). This shift is marked by an increased abundance of bacterial pathogens, including *Pseudomonas aeruginosa*, which is also positively associated with viral RNA load. Additionally, we observe a robust host transcriptional response in the nasal epithelia of CoV^+ patients, indicative of an antiviral innate immune response and neuronal damage. These data suggest that the inflammatory response caused by SARS-CoV-2 infection is associated with an increased abundance of bacterial pathogens in the nasal cavity that could contribute to increased incidence of secondary bacterial infections.

INTRODUCTION

Severe acute respiratory syndrome coronavirus 2 (SARS-CoV-2) is the causative agent of coronavirus disease 2019 (COVID-19) (Zhou et al., 2020b; Zhu et al., 2020), a respiratory disease ranging in clinical presentation from an asymptomatic (~80% of cases) to a fatal infection (~1%–2%) (Guan et al., 2020; Hu et al., 2021). Long-term consequences of COVID-19 range from anosmia and ageusia (Guan et al., 2020; Harrison et al., 2020; Hornuss et al., 2020) to respiratory (e.g., dyspnea) and nervous system (e.g., headache, anosmia) complications (Lopez-Leon et al., 2021). Numerous studies have identified advanced age, obesity, diabetes, and male sex as risk factors for severe COVID-19 (Callender et al., 2020; Ejaz et al., 2020; Harrison et al., 2020; Hu et al., 2021). Other factors, including mucosal microbial defenses and viral burden at the site of initial infection, have been underexplored.

SARS-CoV-2 is primarily spread through the inhalation of virus-laden respiratory droplets (Harrison et al., 2020). Initial entry and subsequent replication occur in the upper respiratory tract (URT) following the interaction of the viral spike protein and host ACE2 (Hoffmann et al., 2020; Murgolo et al., 2021; Shang et al., 2020). The nasal cavity is thought to be the initial site of viral replication rather than the oral cavity due to higher expression of ACE2 (Chen et al., 2020; Sungnak et al., 2020; Zou et al., 2020b) and greater levels of viral RNA (vRNA) at this site (Zou et al., 2020a). Rapid and uncontrolled replication can lead to infection of the lower respiratory tract and severe disease. However, a lack of correlation between disease severity and vRNA load in nasal cavities suggests that other factors contribute to disease outcomes (Lui et al., 2020; Yilmaz et al., 2021; Zou et al., 2020a).

The mucosal microbiome plays a critical role in modulating viral infection (Gallo et al., 2021; He et al., 2020; Khatiwada and Subedi, 2020; Wilks and Golovkina, 2012). Disruption of microbial communities by viral infection can exacerbate inflammation, facilitate coinfection, and deregulate the adaptive immune response (Gallo et al., 2021; He et al., 2020; Khatiwada and Subedi, 2020; Wilks and Golovkina, 2012). Furthermore, severe inflammation in nasal epithelium can lead to short- and long-term symptoms such as anosmia and ageusia (Melo et al., 2021; Rawson and Huang, 2009). However, a limited number of studies have examined the interplay between respiratory microbiome and acute SARS-CoV-2 infection. Studies of nasopharyngeal samples from small cohorts of mild and severe COVID-19 patients show variable differences in diversity and increased abundance of select phyla without accounting for the potential impact of viral load (Butler et al., 2021; De Maio et al., 2020; Nardelli et al., 2021; Rueca et al., 2021). Other studies of bronchoalveolar lavage and pharyngeal samples in severe patients reported a general dysbiosis of the lower respiratory microbiome similar to that of pneumonia patients (Budding et al., 2020; Shen et al., 2020).

Studies aimed at understanding the impact of COVID-19 and viral burden on nasal microbial communities are urgently needed

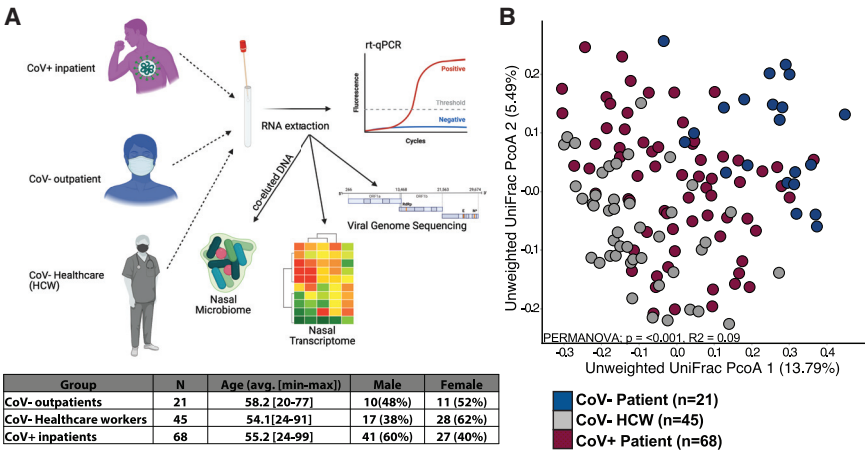

Group	N	Age (avg. [min-max])	Male	Female
CoV- outpatients	21	58.2 [20-77]	10(48%)	11 (52%)
CoV- Healthcare workers	45	54.1[24-91]	17 (38%)	28 (62%)
CoV+ inpatients	68	55.2 [24-99]	41 (60%)	27 (40%)

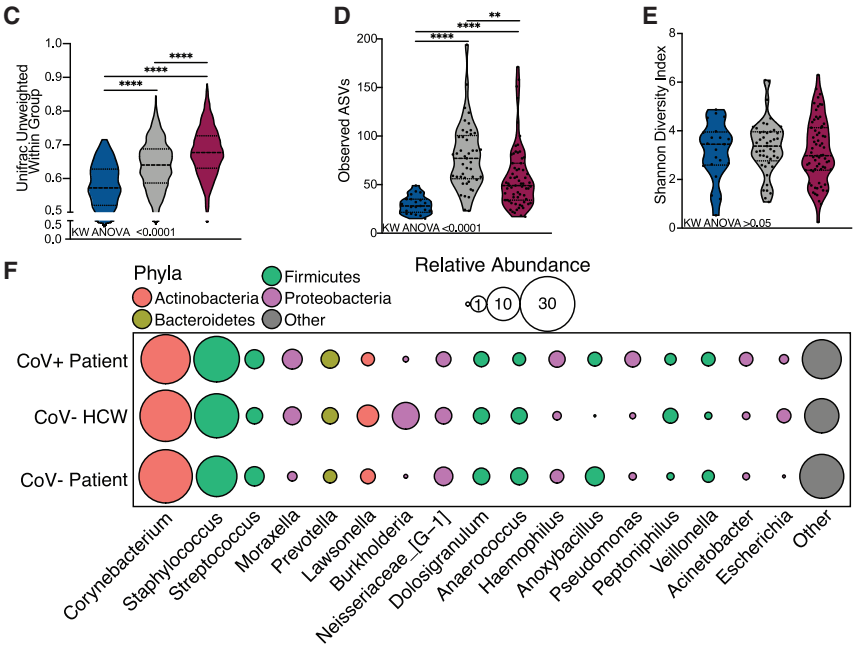

Figure 1. The nasal microbiome of SARS-CoV-2-infected patients is distinct

(A) Study design.

(B) Principal coordinate analysis of nasal microbial communities unweighted UniFrac distance colored by host status. The contribution of host status to the total variance in the unweighted UniFrac dissimilarity was measured using permutational multivariate analysis of variance (PERMANOVA).

(C–E) Violin plot of (C) average unweighted UniFrac distances, (D) number of observed ASVs, and (E) Shannon diversity. Significance for (C)–(E) was determined using a Kruskal-Wallis non-parametric ANOVA (p values inset at the bottom of each panel) with Dunn's multiple comparison. **p < 0.01, **** = p < 0.0001.

(F) Bubble plots of bacterial genera with >1% average abundance across the entire study population. The size of each circle indicates the average relative abundance for each taxa, and the color of each circle denotes bacterial phyla.

See also Figure S1 and Table S1.

RESULTS

SARS-CoV-2 infection is associated with increased abundance of pathobionts in the nasal microbiome

We utilized 16S rRNA gene amplicon sequencing to profile nasal microbiomes from SARS-CoV-2 positive (CoV^+) patients at the time of diagnosis (n = 68), CoV^- outpatients seeking elective procedures (n = 21), and CoV^- healthcare workers (HCWs; n = 45) (Figure 1A). These three groups did not differ by age or sex (Figure 1A; Table S1). We first determined whether microbial DNA co-eluted in vRNA extractions was reflective of a typical nasal microbiome. To that end, we compared our dataset to a previously published healthy nasal microbiome dataset obtained using conventionally DNA extraction methods (De Boeck et al., 2017) (Figure S1B). This analysis revealed a high degree of overlap between the two studies (Figure S1B). Additionally, we found that age and sex explain a significant amount of variation in unweighted and weighted UniFrac distance, respectively (Figures S1C–S1H). However, host CoV status exerted a greater impact on the nasal microbiome composition than did age and sex, accounting for 9.3% of the total variation of unweighted UniFrac distance (Figures 1B, S1G, and S1H).

Additionally, nasal microbial communities in CoV^+ patients showed the highest intra-group variability followed by communities from CoV^- HCWs and CoV^- outpatients (Figure 1C). These same trends held for abundance-based weighted UniFrac distance (Figures S2A and S2B). We also observed an increased richness in nasal community from COV^+ patients to gain insight into acute and long-term consequences of COVID-19. In this study, we determined the impact of acute SARS-CoV-2 infection with a spectrum of vRNA loads on the nasal microbiome, local host transcriptional responses, and potential association with viral genome sequence diversity. Our cross-sectional study of CoV^+ patients, CoV^- outpatients, and CoV^- healthcare workers from the same hospital indicated a distinct shift in the nasal microbiome of patients at the time of COVID-19 diagnosis, featuring the increased abundance of pathobionts such as *Rothia*, *Acinetobacter*, and *Pseudomonas*. This was accompanied by the upregulation of host antiviral genes and the downregulation of genes with roles in mucosal and neuronal cell homeostasis. Overall, our data suggest that SARS-CoV-2 infection is associated with an increased abundance of bacterial pathogens in the nasal cavity and virus-induced host dysregulation at the site of infection.

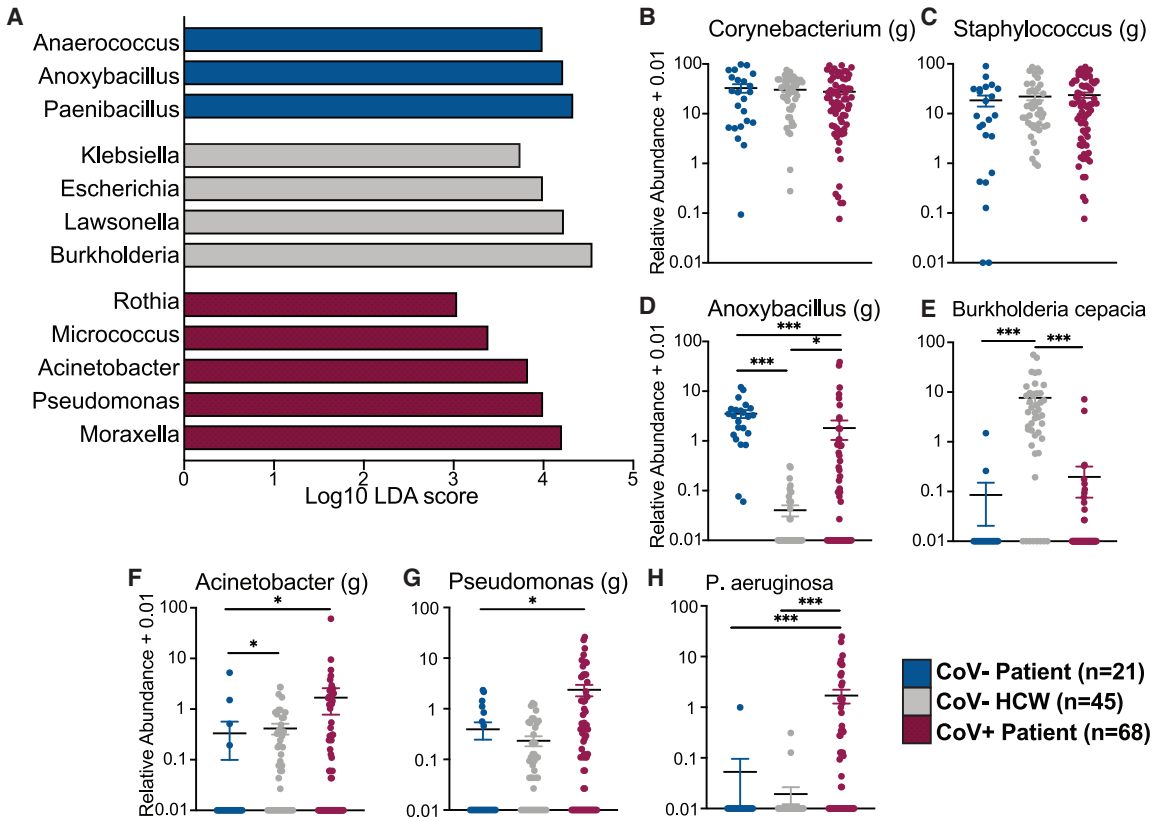

Figure 2. The nasal microbiome of SARS-CoV-2-infected patients and healthcare workers are enriched in opportunistic bacterial pathogens

(A) Selected differentially abundant genera in the nasal microbiome between CoV$^-$, HCWs, and CoV$^+$ individuals. Differential abundance was determined using LEfSe (log_{10} linear discriminant analysis [LDA] score >2).

(B–H) Scatterplots of bacterial genera and species of interest identified by LEfSe analysis plotted as log_{10} relative abundance + 0.01. Horizontal black lines represent the mean and whiskers represent the SEM. Significance for (B)–(H) was determined using a Kruskal-Wallis non-parametric ANOVA, with a Dunn's multiple comparison test. *$p < 0.05$, ***$p < 0.001$.

See also Figure S2 and Table S2.

and HCWs as indicated by a higher number of observed amplicon sequencing variants (ASVs) compared to CoV$^-$ outpatients (Figure 1D). As expected, all three groups had comparable low community Shannon diversity values, indicative of a low-complexity community dominated by a few microbes (Figure 1E). We next probed the taxonomic landscape of the nasal microbiome to identify microbial taxa driving the shift in the overall community. At the phyla level, samples from all groups were dominated by Actinobacteria, Firmicutes, and Proteobacteria (Figures 1F and S2C). Common nasal genera such as *Corynebacterium*, *Staphylococcus*, *Streptococcus*, *Dolosigranulum*, and *Neisseria* were highly abundant in all three groups (Figures 1F and S2C).

Comparison of the three groups using linear discriminant analysis effect size (LEfSe) revealed enrichment of specific genera in each group (Figure 2A; Table S2). Specifically, *Anaerococcus* was enriched in CoV$^-$ outpatients, while *Lawsonella* and *Burkholderia* were most abundant in CoV$^-$ HCWs (Figure 2A; Table S2). Finally, several pathogenic bacteria such as *Rothia*, *Acinetobacter*, and *Pseudomonas* were most abundant in CoV$^+$ patients (Figure 2A; Table S1). To further explore the distribution of specific taxonomic groups, we plotted the abundance of selected taxa. The two dominant genera, *Corynebacterium* and *Staphylococcus*, were equally abundant in the groups (Figures 2B and 2C). Interestingly, abundance of *Anoxybacillus* was higher in both CoV$^-$ outpatients and CoV$^+$ inpatients compared to HCWs (Figure 2D). Conversely, *Burkholderia cepacia* was significantly more abundant in CoV$^-$ HCWs compared to the two patient groups (Figures 1F and 2E). Alternatively, the genera *Acinetobacter* and *Pseudomonas* were most abundant in the CoV$^+$ patients (Figures 2F and 2G). When probed at the species level, *Pseudomonas aeruginosa* was highly enriched in CoV$^+$ patients (Figure 2H). These data suggest that SARS-CoV-2 infection is associated with a shift in the nasal microbiome and acquisition of pathobionts.

Associations between SARS-CoV-2 vRNA load and the nasal microbiome

We next determined whether vRNA load is associated with changes in the nasal microbiome. We divided CoV$^+$ inpatients into three groups based on cycle threshold (Ct) values at

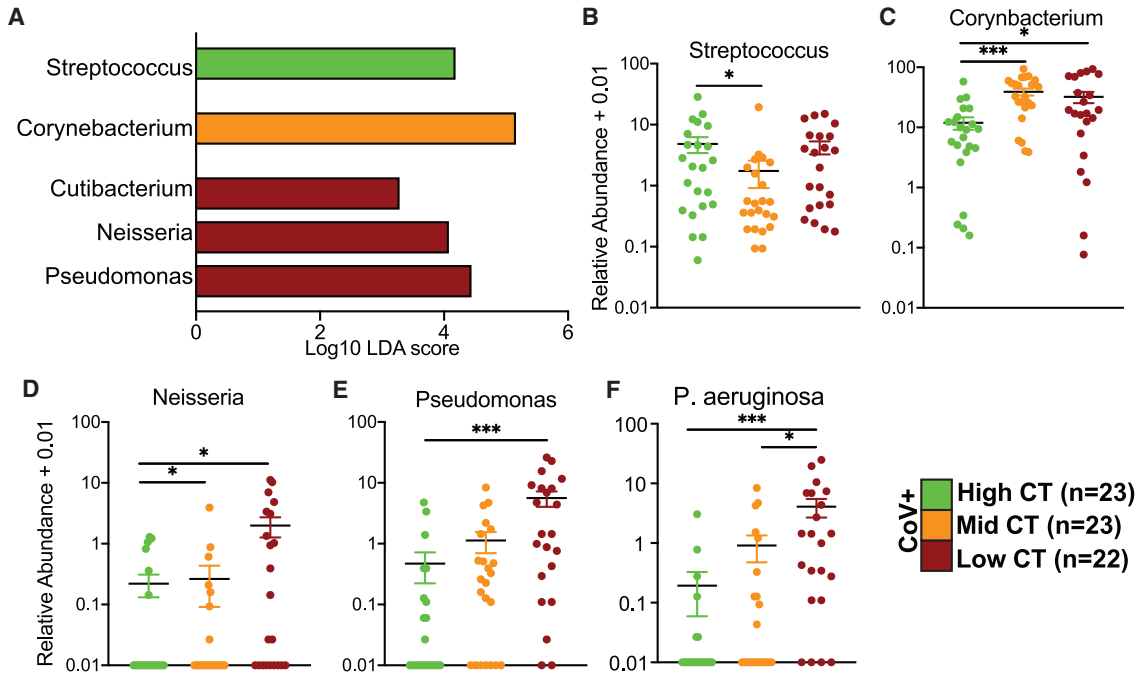

Figure 3. The nasal microbiome of SARS-CoV-2-infected patients is associated with vRNA load

(A) Differentially abundant genera in the nasal microbiome between CoV$^+$ individuals stratified by vRNA load into high, middle, and low Ct. Differential abundance was determined using LEfSe (log_{10} LDA score >2).

(B–F) Scatterplots of bacterial genera and species of interest identified by LEfSe analysis plotted as log_{10} relative abundance + 0.01. Horizontal black bars represent the mean and whiskers represent the SEM. Significance for (B)–(H) was determined using a Kruskal-Wallis non-parametric ANOVA, with Dunn's multiple comparison test. *$p < 0.05$, ***$p < 0.001$.

See also Figure S3.

admission: high Ct value (<40–34.6; n = 23), middle Ct value (32.9–25.0; n = 23), and low Ct value (23.5–15.8; n = 22) (Figure S2D). We compared the number of observed ASVs and community composition based on unweighted and weighted UniFrac distance, as well as intra-group variability across the three Ct groups (Figures S2E–S2I). vRNA load did not impact the diversity of the nasal microbial community (Figures S2E–S2G). However, when the relative abundance of taxa was considered, viral loads explained 10% of the overall community composition (Figure S2H). Moreover, the nasal communities of low and middle Ct groups were comparable to each other and distinct from the high Ct group (Figure S2I), suggesting that shifts in the nasal microbiome are modulated by vRNA load.

LEfSe analysis between the three Ct groups showed higher abundance of *Streptococcus* in nasal microbial communities of patients with high Ct, higher abundance of *Corynebacterium* in patients with middle Ct, and high abundance of *Cutibacterium*, *Neisseria*, and *Pseudomonas* in patients with low Ct (Figure 3A). The relative abundance of the genus *Streptococcus* was highest in the high Ct group (Figure 3B), while that of *Corynebacterium* was more abundant in the middle and low Ct groups (Figure 3C). Finally, *Neisseria* and *Pseudomonas* were more abundant in the low Ct group (Figures 3D and 3E), and *P. aeruginosa* was positively associated with viral loads (Figure 3F).

SAR-CoV-2 infection remodels the nasal epithelium transcriptome

We compared the nasal transcriptomes of a subset of CoV$^-$ HCWs (n = 4) and CoV$^+$ inpatients (n = 4) using RNA sequencing (RNA-seq) (Figure 4). We identified 692 differentially expressed genes (DEGs) in the CoV$^+$ group relative to HCWs (Figure 4A). Upregulated DEGs (n = 377) enriched to multiple Gene Ontology (GO) terms associated with innate and adaptive host defense pathways such as "response to virus," "inflammatory response," "response to bacterium," and "lymphocyte activation" (Figure 4B). A large number of interferon-stimulated (ISGs; e.g., *IFITM3*, *ISG15*) and type I interferon signaling genes (e.g., *IRF7*, *STAT1*) mapped to the GO term "response to virus" (Figure 4C). Genes with roles in nuclear factor κB (NF-κB) and JUN-ATP-1 signaling, such as *BCL3* and *MYD88*, mapped to GO terms "inflammatory response." Expression of genes involved in leukocyte chemotaxis (e.g., *CCL2*, *CCR1*), hematopoiesis (e.g., *CD53*, *IKZF1*), and B cell activation (e.g., *IGHA*, *LCK*) were upregulated in CoV$^+$ patients. Interestingly, genes that encode inhibitory receptors (e.g., *CD300E*, *LAGLS9*) as well as genes involved in cell death (e.g., *BCL2*, *NUPR1*) were also highly upregulated. Additionally, upregulated DEGs (e.g., *SNCA*, *MDK)* belonged to "neuron death" (Figure 4B).

Downregulated DEGs (n = 315) mapped to GO terms related to tissue homeostasis (e.g., "response to wounding"), cellular organization (e.g., "microtubule-based movement"), and neuronal

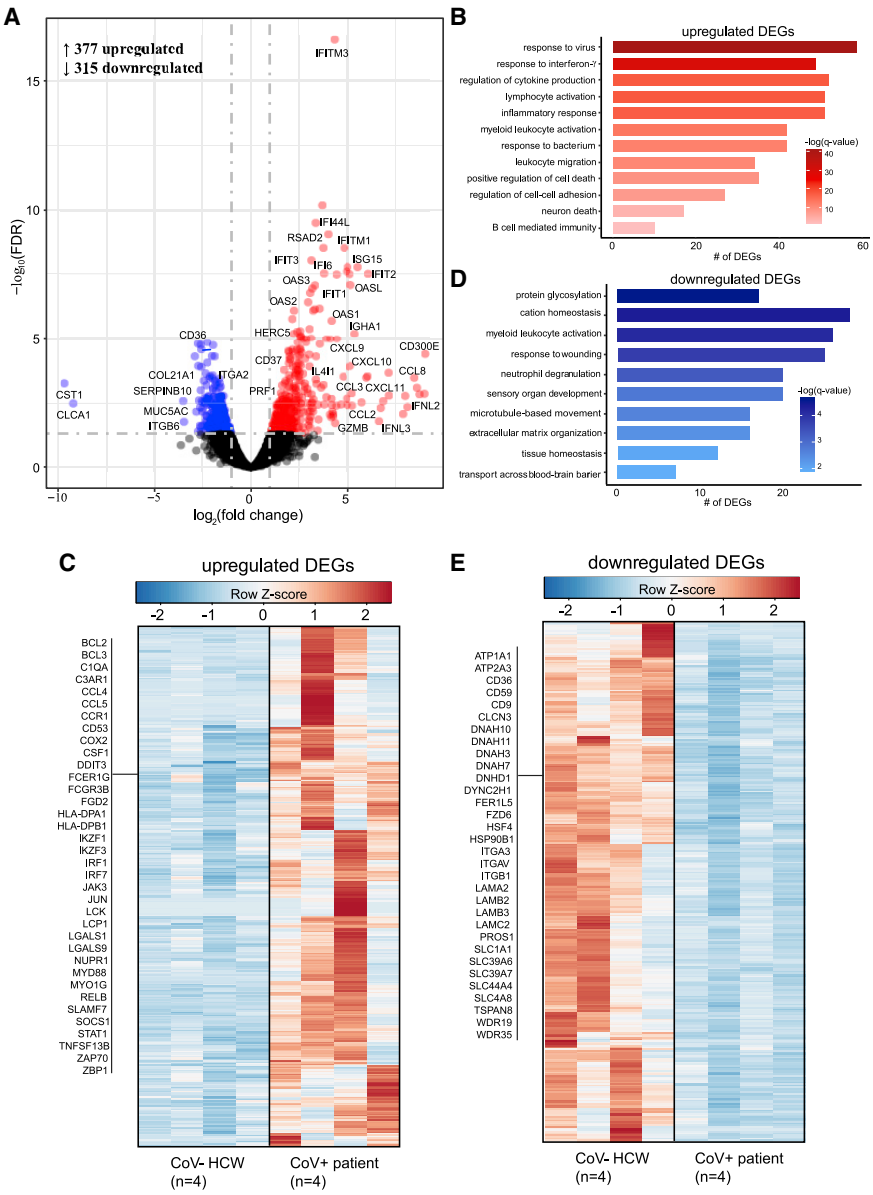

Figure 4. Transcriptional profiling of the nasal passages reveals robust immune activation

(A) Volcano plot of gene expression changes in CoV^{+} patients relative to CoV^{-} HCWs. Upregulated differentially expressed genes (DEGs) are indicated in red; downregulated genes are indicated in blue.

(B) Functional enrichment of upregulated DEGs. Horizontal bars represent the number of genes enriching to each GO term, with color intensity representing the negative log of the false discovery rate (FDR)-adjusted p value (−log[q value]).

(C) Heatmap of upregulated DEGs. Columns of all heatmaps represent the RPKM (reads per kilobase transcript per million mapped reads) of one individual. Range of colors per each heatmap is based on scaled and centered RPKM values of the represented DEGs (red indicates upregulated; blue indicates downregulated).

(D) Functional enrichment of downregulated DEGs as described in (C).

(E) Heatmap of downregulated DEGs. See (D) for additional details.

processes (e.g., "sensory organ development") (Figure 4C). Notable downregulated DEGs encoded integrins (e.g., *ITGA2/3/V*, *ITGB1/6*), laminins (e.g., *LAMA2/B2/B3/C2*), and microtubules (e.g., *DNAH3/7/10/11*, *DYNC2H1*) comprising intracellular and extracellular structures such as cilia and cell-cell adhesion junctions. Genes associated with mucin production in nasal passages (e.g., *MUC20*, *MUC5AC*) were downregulated. Finally, genes encoding ion channels important for chloride ion balance and neuron homeostasis (e.g., *ATP1A1*, *SLC39A*, *CLCN3*) were downregulated (Figures 4A and 4E).

Viral genome recovery, but not genetics, correlates with viral loads

To identify associations between vRNA load, genome recovery, and viral evolution, we assembled SARS-CoV-2 genomes from CoV^{+} patients. As expected, the Ct value was negatively associated with viral genome coverage (Pearson correlation, r = −0.509, p = 0.0001), with 81.6%, 54.58%, and 8.3% of genomes from low, middle, and high Ct groups having greater than 90% genome coverage, respectively. All genomes with adequate coverage harbored the spike D614G and nsp12 P4715L mutations, a noncoding mutation in the 5′ UTR, and a synonymous mutation in nsp3 (F924) (Figure S3A). The nucleoprotein T205I mutation associated with the 501.V2 variant was found in two low and middle Ct samples. Genomes belonged to three main clades, that is, 20A, 20B, and 20C, with very few sequences belonging to the 20H clade, which emerged in October and no distinct relationship to current variants of concern (P.1, B.1.1.7, B.1.351, B.1.427, B.1.429) or partitioning according to Ct value (Figure S3B).

DISCUSSION

In this study, we explored connections between acute SARS-CoV-2 infection, the nasal microbiome, and the local host transcriptional response. While a wealth of studies have focused on the systemic host response to SARS-CoV-2, few studies have investigated the impact of acute SARS-CoV-2 on the nasal epithelium. SARS-CoV-2 infection occurs primarily via respiratory droplets, with the initial viral replication taking place in the nasal epithelia (Murgolo et al., 2021; Sungnak et al., 2020).

Most individuals who contract SARS-CoV-2 clear infection within the URT, resulting in asymptomatic to mild disease (Guan et al., 2020). When this initial response is insufficient, SARS-CoV-2 migrates into the lower respiratory tract, leading to moderate/severe COVID-19 characterized by acute respiratory distress syndrome, pneumonias, and cytokine storm (Hu et al., 2021; Kuri-Cervantes et al., 2020; Grasselli et al., 2021; Guan et al., 2020). Thus, there is a clear need to understand the host and microbial factors in the nasal cavity during acute infection.

The healthy nasal microbiome is dominated by *Corynebacterium*, *Staphylococcus*, *Streptococcus*, *Dolosigranulum*, and *Moraxella* (Whelan et al., 2014; Bassis et al., 2014; Stearns et al., 2015). This community is influenced by a multitude of external factors such as age, sex, antibiotic use, and pollutants (Wos-Oxley et al., 2010; Charlson et al., 2010; Ramakrishnan et al., 2018). Sex and age exerted a limited effect on the overall composition of the nasal microbiome compared to SARS-CoV-2 infection. However, we were unable to control for antibiotic use, exposure to pollutants, socioeconomic status, and race, all of which could differ considerably between the groups given the high prevalence of COVID-19 in Hispanic patients with lower socioeconomic status in Orange County (Khanijahani, 2021; Hatef et al., 2020). The composition of the nasal microbiome can impact host susceptibility and disease course following respiratory infection (Teo et al., 2015; Lee et al., 2019). In turn, acute viral infections can modulate bacterial communities potentially favoring the expansion of opportunistic pathogens (Edouard et al., 2018; Wolter et al., 2014). In this study, we show that the nasal microbiome of CoV^+ patients was enriched in pathogenic bacteria such *Acinetobacter*, *Rothia*, *Moraxella*, and *P. aeruginosa.* Similarly, an increased abundance of *Pseudomonas* was also observed following influenza A infection and in throat samples collected from COVID-19 patients (Xu et al., 2021; Kaul et al., 2020). However, the cross-sectional nature of our study makes it impossible to determine whether viral infection alters the nasal microbiome or whether the nasal microbiome community state type pre-disposes an individual to viral infection. A recent longitudinal study found that rhinovirus infection did not significantly alter the nasal microbiome, but individuals with a *Pseudomonas*-dominated community prior to infection experienced more severe symptoms (Lehtinen et al., 2018). Therefore, high abundance of *Pseudomonas* in the nasal microbiome may predispose the host to severe respiratory viral infection. Our findings are in line with increased risk of secondary bacterial infections in COVID-19 patients, especially those who are severely ill (Feng et al., 2020; Vaillancourt and Jorth, 2020; Zhou et al., 2020a).

Hospital acquired infections (HAIs) are a major public health concern. Indeed, up to 46% of patients hospitalized with COVID-19 suffered from a HAI (Grasselli et al., 2021). One of the major reservoirs for opportunistic pathogens is the nasal cavity, which can act as the entry point and contribute to the spread of bacterial infections to the rest of the respiratory tract (Dimitri-Pinheiro et al., 2020). HCWs are often carriers of pathogens associated with nosocomial infection such as methicillin-resistant *Staphylococcus aureus* (MRSA) given their extended exposure to the hospital environment (El Aila et al., 2017). Our analysis found an enrichment of pathobionts such as *B. cepacia*, often detected in patients with underlying conditions such as cystic fibrosis (Coutinho et al., 2011; Kalish et al., 2006) and the elderly (El Chakhtoura et al., 2017), in the nasal communities of HCWs. The abundance of *Acinetobacter* was significantly higher in HCWs and CoV^+ patients compared to CoV^- outpatients. Since CoV^+ samples were collected at hospital admission, it is possible that patients with respiratory infections are contributing to the high prevalence of bacterial pathogens in the hospital environment, which is being reflected in the nasal microbiome of HCWs. Additionally, *Rothia* was more abundant in the nasal microbiome of CoV^+ patients. Interestingly, a recent study found that *Rothia* was the best predictor of detectable SARS-CoV-2 vRNA in patient samples and on the surfaces of COVID-19 patient rooms (Marotz et al., 2021).

We also profiled the host transcriptional profile of the nasal epithelium in a subset of patients. As recently described (Butler et al., 2021; Islam et al., 2021; Lieberman et al., 2020; Ng et al., 2021), we observed an upregulation of genes associated with innate immune cell activation, antiviral defense, inflammation, and cell death. Furthermore, the upregulation of genes associated with neuronal death and the downregulation of genes influencing epithelial integrity and sensory organ development support a mechanism for infection-induced anosmia and ageusia (de Melo et al., 2021; Melo et al., 2021; Rawson and Huang, 2009).

Additionally, we sought to determine the relationship between vRNA load, viral phylogeny, and viral genome recovery. Consistent with previous studies, genome recovery was negatively correlated with Ct value (La Scola et al., 2020; Bullard et al., 2020; Singanayagam et al., 2020). We detected the D614G amino acid change in all samples, which is expected given the global dominance of this genotype (Korber et al., 2020; Isabel et al., 2020). Mutations in the RDRP subunits nsp12 and nsp3, which could impact viral replication and immune evasion and immune antagonist, were also present in all samples (Brosey et al., 2021; Hillen et al., 2020). Given the limited viral genetic diversity we observed within our study population, we were unable to determine the impact of viral genetic variation on the composition of the nasal microbiome or host transcriptional response.

In summary, data presented herein show that SARS-CoV-2 infection is associated with a distinct shift in the composition of the nasal microbiome, including an increased abundance of bacterial pathogens such as *P. aeruginosa*. Additionally, HCW nasal microbiomes are enriched in pathogens known to cause nosocomial infections such as *B. cepacia*. Transcriptional profiling indicated a robust local immune response to SARS-CoV-2 infection and provided support for neuronal damage in the URT leading to anosmia. This study had some limitations. The samples used in this study were initially collected for SARS-CoV-2 diagnosis and were therefore not processed in the typical fashion for either host transcriptomics or microbiome analysis. Additionally, our study consisted of only one time point. A longitudinal study should be performed to gain much needed insight into the dynamic changes in microbial communities and host responses within the nasal cavity. Finally, analysis of samples from individuals with asymptomatic infection would provide additional valuable insight into the determinants of disease.

STAR★METHODS

Detailed methods are provided in the online version of this paper and include the following:

- KEY RESOURCES TABLE
- RESOURCE AVAILABILITY
  - Lead contact
  - Materials availability
  - Data and code availability
- EXPERIMENTAL MODEL AND SUBJECT DETAILS
  - Human subjects
- METHOD DETAILS
  - Sample collection, extraction, and SARS-CoV-2 RNA quantification
  - 16S amplicon libraries construction and data analysis
  - RNA-seq library preparation and analysis
  - SARS-CoV-2 genome library construction and analysis
- QUANTIFICATION AND STATISTICAL ANALYSIS

SUPPLEMENTAL INFORMATION

Supplemental information can be found online at https://doi.org/10.1016/j.celrep.2021.109637.

ACKNOWLEDGMENTS

This study was supported by NIH grants UL1 TR001414, 1R01AI152258-02, and 3R01AA028735-01S1. N.S.R. is supported by NIH T32 AI007319. The content is solely the responsibility of the authors and does not necessarily represent the official views of the NIH. Experimental design and graphical abstract figures were generated using graphics from BioRender.com. We thank the Chao Family Comprehensive Cancer Center (P30CA062203) for providing the de-identified biospecimens used in this study.

AUTHOR CONTRIBUTIONS

N.S.R. and I.M. conceived and designed the experiments. N.S.R., A.N.P., A.N.M., B.M.D., A.J., and I.R.C. performed the experiments. N.S.R, A.N.P., and A.N.M. analyzed the data. N.S.R., A.N.P., and I.M. interpreted the results and wrote the paper. All authors have read and approved the final draft of the manuscript.

DECLARATION OF INTERESTS

The authors declare no competing interests.

Received: May 26, 2021
Revised: July 12, 2021
Accepted: August 6, 2021
Published: August 13, 2021

REFERENCES

Bassis, C.M., Tang, A.L., Young, V.B., and Pynnonen, M.A. (2014). The nasal cavity microbiota of healthy adults. Microbiome *2*, 27.

Bolyen, E., Rideout, J.R., Dillon, M.R., Bokulich, N.A., Abnet, C.C., Al-Ghalith, G.A., Alexander, H., Alm, E.J., Arumugam, M., Asnicar, F., et al. (2019). Reproducible, interactive, scalable and extensible microbiome data science using QIIME 2. Nat. Biotechnol. *37*, 852–857.

Brosey, C.A., Houl, J.H., Katsonis, P., Balapiti-Modarage, L.P.F., Bommagani, S., Arvai, A., Moiani, D., Bacolla, A., Link, T., Warden, L.S., et al. (2021). Targeting SARS-CoV-2 Nsp3 macrodomain structure with insights from human poly(ADP-ribose) glycohydrolase (PARG) structures with inhibitors. Prog. Biophys. Mol. Biol. *163*, 171–186.

Budding, A., Sieswerda, E., Wintermans, B., and Bos, M. (2020). An age dependent pharyngeal microbiota signature associated with Sars-Cov-2 infection. https://ssrn.com/abstract=3582780.

Bullard, J., Dust, K., Funk, D., Strong, J.E., Alexander, D., Garnett, L., Boodman, C., Bello, A., Hedley, A., Schiffman, Z., et al. (2020). predicting infectious severe acute respiratory syndrome coronavirus 2 from diagnostic samples. Clin. Infect. Dis. *71*, 2663–2666.

Butler, D., Mozsary, C., Meydan, C., Foox, J., Rosiene, J., Shaiber, A., Danko, D., Afshinnekoo, E., MacKay, M., Sedlazeck, F.J., et al. (2021). Shotgun transcriptome, spatial omics, and isothermal profiling of SARS-CoV-2 infection reveals unique host responses, viral diversification, and drug interactions. Nat. Commun. *12*, 1660.

Callahan, B.J., McMurdie, P.J., Rosen, M.J., Han, A.W., Johnson, A.J., and Holmes, S.P. (2016). DADA2: High-resolution sample inference from Illumina amplicon data. Nat. Methods *13*, 581–583.

Callender, L.A., Curran, M., Bates, S.M., Mairesse, M., Weigandt, J., and Betts, C.J. (2020). The impact of pre-existing comorbidities and therapeutic interventions on COVID-19. Front. Immunol. *11*, 1991.

Charlson, E.S., Chen, J., Custers-Allen, R., Bittinger, K., Li, H., Sinha, R., Hwang, J., Bushman, F.D., and Collman, R.G. (2010). Disordered microbial communities in the upper respiratory tract of cigarette smokers. PLoS ONE *5*, e15216.

Chen, M., Shen, W., Rowan, N.R., Kulaga, H., Hillel, A., Ramanathan, M., Jr., and Lane, A.P. (2020). Elevated ACE2 expression in the olfactory neuroepithelium: Implications for anosmia and upper respiratory SARS-CoV-2 entry and replication. bioRxiv. https://doi.org/10.1101/2020.05.08.084996.

Coutinho, C.P., Dos Santos, S.C., Madeira, A., Mira, N.P., Moreira, A.S., and Sá-Correia, I. (2011). Long-term colonization of the cystic fibrosis lung by *Burkholderia cepacia* complex bacteria: Epidemiology, clonal variation, and genome-wide expression alterations. Front. Cell. Infect. Microbiol. *1*, 12.

De Boeck, I., Wittouck, S., Wuyts, S., Oerlemans, E.F.M., van den Broek, M.F.L., Vandenheuvel, D., Vanderveken, O., and Lebeer, S. (2017). Comparing the healthy nose and nasopharynx microbiota reveals continuity as well as niche-specificity. Front. Microbiol. *8*, 2372.

De Maio, F., Posteraro, B., Ponziani, F.R., Cattani, P., Gasbarrini, A., and Sanguinetti, M. (2020). Nasopharyngeal microbiota profiling of SARS-CoV-2 infected patients. Biol. Proced. Online *22*, 18.

de Melo, G.D., Lazarini, F., Levallois, S., Hautefort, C., Michel, V., Larrous, F., Verillaud, B., Aparicio, C., Wagner, S., Gheusi, G., et al. (2021). COVID-19-related anosmia is associated with viral persistence and inflammation in human olfactory epithelium and brain infection in hamsters. Sci. Transl. Med. *13*, eabf8396.

Dimitri-Pinheiro, S., Soares, R., and Barata, P. (2020). The microbiome of the nose—Friend or foe? Allergy Rhinol. (Providence) *11*, 2152656720911605.

Dixon, P. (2003). VEGAN, a package of R functions for community ecology. J. Vegetation Sci. *14*, 927–930.

Edouard, S., Million, M., Bachar, D., Dubourg, G., Michelle, C., Ninove, L., Charrel, R., and Raoult, D. (2018). The nasopharyngeal microbiota in patients with viral respiratory tract infections is enriched in bacterial pathogens. Eur. J. Clin. Microbiol. Infect. Dis. *37*, 1725–1733.

Ejaz, H., Alsrhani, A., Zafar, A., Javed, H., Junaid, K., Abdalla, A.E., Abosalif, K.O.A., Ahmed, Z., and Younas, S. (2020). COVID-19 and comorbidities: Deleterious impact on infected patients. J. Infect. Public Health *13*, 1833–1839.

El Aila, N.A., Al Laham, N.A., and Ayesh, B.M. (2017). Nasal carriage of methicillin resistant *Staphylococcus aureus* among health care workers at Al Shifa hospital in Gaza Strip. BMC Infect. Dis. *17*, 28.

El Chakhtoura, N.G., Saade, E., Wilson, B.M., Perez, F., Papp-Wallace, K.M., and Bonomo, R.A. (2017). A 17-year nationwide study of *Burkholderia cepacia* complex bloodstream infections among patients in the united states veterans health administration. Clin. Infect. Dis. *65*, 1253–1259.

Escapa, I.F., Chen, T., Huang, Y., Gajare, P., Dewhirst, F.E., and Lemon, K.P. (2018). New insights into human nostril microbiome from the expanded Human Oral Microbiome Database (eHOMD): A resource for the microbiome of the human aerodigestive tract. mSystems *3*, e00187-18.

Feng, Y., Ling, Y., Bai, T., Xie, Y., Huang, J., Li, J., Xiong, W., Yang, D., Chen, R., Lu, F., et al. (2020). COVID-19 with different severities: A multicenter study of clinical features. Am. J. Respir. Crit. Care Med. *201*, 1380–1388.

Gallo, O., Locatello, L.G., Mazzoni, A., Novelli, L., and Annunziato, F. (2021). The central role of the nasal microenvironment in the transmission, modulation, and clinical progression of SARS-CoV-2 infection. Mucosal Immunol. *14*, 305–316.

Grasselli, G., Scaravilli, V., Mangioni, D., Scudeller, L., Alagna, L., Bartoletti, M., Bellani, G., Biagioni, E., Bonfanti, P., Bottino, N., et al. (2021). Hospital-acquired infections in critically ill patients with COVID-19. Chest *160*, 454–465.

Guan, W.-J., Ni, Z.-Y., Hu, Y., Liang, W.-H., Ou, C.-Q., He, J.-X., Liu, L., Shan, H., Lei, C.-L., Hui, D.S.C., et al.; China Medical Treatment Expert Group for Covid-19 (2020). Clinical characteristics of coronavirus disease 2019 in China. N. Engl. J. Med. *382*, 1708–1720.

Backman, T.W., and Girke, T. (2016). systemPipeR: NGS workflow and report generation environment. BMC Bioinformatics *17*, 388.

Harrison, A.G., Lin, T., and Wang, P. (2020). Mechanisms of SARS-CoV-2 transmission and pathogenesis. Trends Immunol. *41*, 1100–1115.

Hatef, E., Chang, H.Y., Kitchen, C., Weiner, J.P., and Kharrazi, H. (2020). Assessing the impact of neighborhood socioeconomic characteristics on COVID-19 prevalence across seven states in the United States. Front. Public Health *8*, 571808.

He, Y., Wang, J., Li, F., and Shi, Y. (2020). Main clinical features of COVID-19 and potential prognostic and therapeutic value of the microbiota in SARS-CoV-2 infections. Front. Microbiol. *11*, 1302.

Hillen, H.S., Kokic, G., Farnung, L., Dienemann, C., Tegunov, D., and Cramer, P. (2020). Structure of replicating SARS-CoV-2 polymerase. Nature *584*, 154–156.

Hoffmann, M., Kleine-Weber, H., Schroeder, S., Krüger, N., Herrler, T., Erichsen, S., Schiergens, T.S., Herrler, G., Wu, N.-H., Nitsche, A., et al. (2020). SARS-CoV-2 cell entry depends on ACE2 and TMPRSS2 and is blocked by a clinically proven protease inhibitor. Cell *181*, 271–280.e8.

Hornuss, D., Lange, B., Schröter, N., Rieg, S., Kern, W.V., and Wagner, D. (2020). Anosmia in COVID-19 patients. Clin. Microbiol. Infect. *26*, 1426–1427.

Hu, B., Guo, H., Zhou, P., and Shi, Z.-L. (2021). Characteristics of SARS-CoV-2 and COVID-19. Nat. Rev. Microbiol. *19*, 141–154.

Isabel, S., Graña-Miraglia, L., Gutierrez, J.M., Bundalovic-Torma, C., Groves, H.E., Isabel, M.R., Eshaghi, A., Patel, S.N., Gubbay, J.B., Poutanen, T., et al. (2020). Evolutionary and structural analyses of SARS-CoV-2 D614G spike protein mutation now documented worldwide. Sci. Rep. *10*, 14031.

Islam, A.B.M.M.K., Khan, M.A., Ahmed, R., Hossain, M.S., Kabir, S.M.T., Islam, M.S., and Siddiki, A.M.A.M.Z. (2021). Transcriptome of nasopharyngeal samples from COVID-19 patients and a comparative analysis with other SARS-CoV-2 infection models reveal disparate host responses against SARS-CoV-2. J. Transl. Med. *19*, 32.

Kalish, L.A., Waltz, D.A., Dovey, M., Potter-Bynoe, G., McAdam, A.J., Lipuma, J.J., Gerard, C., and Goldmann, D. (2006). Impact of *Burkholderia dolosa* on lung function and survival in cystic fibrosis. Am. J. Respir. Crit. Care Med. *173*, 421–425.

Katoh, K., and Standley, D.M. (2013). MAFFT multiple sequence alignment software version 7: Improvements in performance and usability. Mol. Biol. Evol. *30*, 772–780.

Kaul, D., Rathnasinghe, R., Ferres, M., Tan, G.S., Barrera, A., Pickett, B.E., Methe, B.A., Das, S.R., Budnik, I., Halpin, R.A., et al. (2020). Microbiome disturbance and resilience dynamics of the upper respiratory tract during influenza A virus infection. Nat. Commun. *11*, 2537.

Khanijahani, A. (2021). Racial, ethnic, and socioeconomic disparities in confirmed COVID-19 cases and deaths in the United States: A county-level analysis as of November 2020. Ethn. Health *26*, 22–35.

Khatiwada, S., and Subedi, A. (2020). Lung microbiome and coronavirus disease 2019 (COVID-19): Possible link and implications. Hum. Microb. J. *17*, 100073.

Korber, B., Fischer, W.M., Gnanakaran, S., Yoon, H., Theiler, J., Abfalterer, W., Hengartner, N., Giorgi, E.E., Bhattacharya, T., Foley, B., et al.; Sheffield COVID-19 Genomics Group (2020). Tracking changes in SARS-CoV-2 spike: Evidence that D614G increases infectivity of the COVID-19 virus. Cell *182*, 812–827.e19.

Kuri-Cervantes, L., Pampena, M.B., Meng, W., Rosenfeld, A.M., Ittner, C.A.G., Weisman, A.R., Agyekum, R.S., Mathew, D., Baxter, A.E., Vella, L.A., et al. (2020). Comprehensive mapping of immune perturbations associated with severe COVID-19. Sci. Immunol. *5*, eabd7114.

La Scola, B., Le Bideau, M., Andreani, J., Hoang, V.T., Grimaldier, C., Colson, P., Gautret, P., and Raoult, D. (2020). Viral RNA load as determined by cell culture as a management tool for discharge of SARS-CoV-2 patients from infectious disease wards. Eur. J. Clin. Microbiol. Infect. Dis. *39*, 1059–1061.

Lee, K.H., Gordon, A., Shedden, K., Kuan, G., Ng, S., Balmaseda, A., and Foxman, B. (2019). The respiratory microbiome and susceptibility to influenza virus infection. PLoS ONE *14*, e0207898.

Lehtinen, M.J., Hibberd, A.A., Männikkö, S., Yeung, N., Kauko, T., Forssten, S., Lehtoranta, L., Lahtinen, S.J., Stahl, B., Lyra, A., and Turner, R.B. (2018). Nasal microbiota clusters associate with inflammatory response, viral load, and symptom severity in experimental rhinovirus challenge. Sci. Rep. *8*, 11411.

Lieberman, N.A.P., Peddu, V., Xie, H., Shrestha, L., Huang, M.L., Mears, M.C., Cajimat, M.N., Bente, D.A., Shi, P.Y., Bovier, F., et al. (2020). In vivo antiviral host transcriptional response to SARS-CoV-2 by viral load, sex, and age. PLoS Biol. *18*, e3000849.

Lopez-Leon, S., Wegman-Ostrosky, T., Perelman, C., Sepulveda, R., Rebolledo, P., Cuapio, A., and Villapol, S. (2021). More than 50 long-term effects of COVID-19: A systematic review and meta-analysis. Sci. Rep. *11*, 16144.

Lozupone, C., Lladser, M.E., Knights, D., Stombaugh, J., and Knight, R. (2011). UniFrac: An effective distance metric for microbial community comparison. ISME J. *5*, 169–172.

Lui, G., Ling, L., Lai, C.K.C., Tso, E.Y.K., Fung, K.S.C., Chan, V., Ho, T.H.Y., Luk, F., Chen, Z., Ng, J.K.C., et al. (2020). Viral dynamics of SARS-CoV-2 across a spectrum of disease severity in COVID-19. J. Infect. *81*, 318–356.

Marotz, C., Belda-Ferre, P., Ali, F., Das, P., Huang, S., Cantrell, K., Jiang, L., Martino, C., Diner, R.E., Rahman, G., et al. (2021). SARS-CoV-2 detection status associates with bacterial community composition in patients and the hospital environment. Microbiome *9*, 132.

Melo, G.D.D., Lazarini, F., Levallois, S., Hautefort, C., Michel, V., Larrous, F., Verillaud, B., Aparicio, C., Wagner, S., Gheusi, G., et al. (2021). COVID-19-related anosmia is associated with viral persistence and inflammation in human olfactory epithelium and brain infection in hamsters. Sci. Transl. Med. *13*, eabf8396.

Murgolo, N., Therien, A.G., Howell, B., Klein, D., Koeplinger, K., Lieberman, L.A., Adam, G.C., Flynn, J., McKenna, P., Swaminathan, G., et al. (2021). SARS-CoV-2 tropism, entry, replication, and propagation: Considerations for drug discovery and development. PLoS Pathog. *17*, e1009225.

Nardelli, C., Gentile, I., Setaro, M., Di Domenico, C., Pinchera, B., Buonomo, A.R., Zappulo, E., Scotto, R., Scaglione, G.L., Castaldo, G., and Capoluongo, E. (2021). Nasopharyngeal microbiome signature in COVID-19 positive patients: Can we definitively get a role to *Fusobacterium periodonticum*? Front. Cell. Infect. Microbiol. *11*, 625581.

Ng, D.L., Granados, A.C., Santos, Y.A., Servellita, V., Goldgof, G.M., Meydan, C., Sotomayor-Gonzalez, A., Levine, A.G., Balcerek, J., Han, L.M., et al. (2021). A diagnostic host response biosignature for COVID-19 from RNA profiling of nasal swabs and blood. Sci. Adv. *7*, eabe5984.

Price, M.N., Dehal, P.S., and Arkin, A.P. (2010). FastTree 2—Approximately maximum-likelihood trees for large alignments. PLoS ONE *5*, e9490.

Quast, C., Pruesse, E., Yilmaz, P., Gerken, J., Schweer, T., Yarza, P., Peplies, J., and Glöckner, F.O. (2013). The SILVA ribosomal RNA gene database

project: Improved data processing and web-based tools. Nucleic Acids Res. *41*, D590–D596.

Ramakrishnan, V.R., Holt, J., Nelson, L.F., Ir, D., Robertson, C.E., and Frank, D.N. (2018). Determinants of the nasal microbiome: Pilot study of effects of intranasal medication use. Allergy Rhinol. (Providence) *9*, 2152656718789519.

Rawson, N.E., and Huang, L. (2009). Impact of oronasal inflammation on taste and smell: An introduction. Ann. N Y Acad. Sci. *1170*, 581–584.

Rhoades, N., Barr, T., Hendrickson, S., Prongay, K., Haertel, A., Gill, L., Garzel, L., Whiteson, K., Slifka, M., and Messaoudi, I. (2019). Maturation of the infant rhesus macaque gut microbiome and its role in the development of diarrheal disease. Genome Biol. *20*, 173.

Rueca, M., Fontana, A., Bartolini, B., Piselli, P., Mazzarelli, A., Copetti, M., Binda, E., Perri, F., Gruber, C.E.M., Nicastri, E., et al. (2021). Investigation of nasal/oropharyngeal microbial community of COVID-19 patients by 16S rDNA sequencing. Int. J. Environ. Res. Public Health *18*, 2174.

Segata, N., Izard, J., Waldron, L., Gevers, D., Miropolsky, L., Garrett, W.S., and Huttenhower, C. (2011). Metagenomic biomarker discovery and explanation. Genome Biol. *12*, R60.

Shang, J., Wan, Y., Luo, C., Ye, G., Geng, Q., Auerbach, A., and Li, F. (2020). Cell entry mechanisms of SARS-CoV-2. Proc. Natl. Acad. Sci. USA *117*, 11727–11734.

Shen, Z., Xiao, Y., Kang, L., Ma, W., Shi, L., Zhang, L., Zhou, Z., Yang, J., Zhong, J., Yang, D., et al. (2020). Genomic diversity of severe acute respiratory syndrome-coronavirus 2 in patients with coronavirus disease 2019. Clin. Infect. Dis. *71*, 713–720.

Singanayagam, A., Patel, M., Charlett, A., Lopez Bernal, J., Saliba, V., Ellis, J., Ladhani, S., Zambon, M., and Gopal, R. (2020). Duration of infectiousness and correlation with RT-PCR cycle threshold values in cases of COVID-19, England, January to May 2020. Euro Surveill. *25*, 2001483.

Stearns, J.C., Davidson, C.J., McKeon, S., Whelan, F.J., Fontes, M.E., Schryvers, A.B., Bowdish, D.M., Kellner, J.D., and Surette, M.G. (2015). Culture and molecular-based profiles show shifts in bacterial communities of the upper respiratory tract that occur with age. ISME J. *9*, 1246–1259.

Sungnak, W., Huang, N., Bécavin, C., Berg, M., Queen, R., Litvinukova, M., Talavera-López, C., Maatz, H., Reichart, D., Sampaziotis, F., et al.; HCA Lung Biological Network (2020). SARS-CoV-2 entry factors are highly expressed in nasal epithelial cells together with innate immune genes. Nat. Med. *26*, 681–687.

Teo, S.M., Mok, D., Pham, K., Kusel, M., Serralha, M., Troy, N., Holt, B.J., Hales, B.J., Walker, M.L., Hollams, E., et al. (2015). The infant nasopharyngeal microbiome impacts severity of lower respiratory infection and risk of asthma development. Cell Host Microbe *17*, 704–715.

Vaillancourt, M., and Jorth, P. (2020). The unrecognized threat of secondary bacterial infections with COVID-19. MBio *11*, e01806-20.

Whelan, F.J., Verschoor, C.P., Stearns, J.C., Rossi, L., Luinstra, K., Loeb, M., Smieja, M., Johnstone, J., Surette, M.G., and Bowdish, D.M. (2014). The loss of topography in the microbial communities of the upper respiratory tract in the elderly. Ann. Am. Thorac. Soc. *11*, 513–521.

Wilks, J., and Golovkina, T. (2012). Influence of microbiota on viral infections. PLoS Pathog. *8*, e1002681.

Wolter, N., Tempia, S., Cohen, C., Madhi, S.A., Venter, M., Moyes, J., Walaza, S., Malope-Kgokong, B., Groome, M., du Plessis, M., et al. (2014). High nasopharyngeal pneumococcal density, increased by viral coinfection, is associated with invasive pneumococcal pneumonia. J. Infect. Dis. *210*, 1649–1657.

Wos-Oxley, M.L., Plumeier, I., von Eiff, C., Taudien, S., Platzer, M., Vilchez-Vargas, R., Becker, K., and Pieper, D.H. (2010). A poke into the diversity and associations within human anterior nare microbial communities. ISME J. *4*, 839–851.

Xu, R., Lu, R., Zhang, T., Wu, Q., Cai, W., Han, X., Wan, Z., Jin, X., Zhang, Z., and Zhang, C. (2021). Temporal association between human upper respiratory and gut bacterial microbiomes during the course of COVID-19 in adults. Commun. Biol. *4*, 240.

Yilmaz, A., Marklund, E., Andersson, M., Nilsson, S., Andersson, L.-M., Lindh, M., and Gisslén, M. (2021). Upper respiratory tract levels of severe acute respiratory syndrome coronavirus 2 RNA and duration of viral RNA shedding do not differ between patients with mild and severe/critical coronavirus disease 2019. J. Infect. Dis. *223*, 15–18.

Zhou, Y., Zhou, B., Pache, L., Chang, M., Khodabakhshi, A.H., Tanaseichuk, O., Benner, C., and Chanda, S.K. (2019). Metascape provides a biologist-oriented resource for the analysis of systems-level datasets. Nat. Commun. *10*, 1523.

Zhou, F., Yu, T., Du, R., Fan, G., Liu, Y., Liu, Z., Xiang, J., Wang, Y., Song, B., Gu, X., et al. (2020a). Clinical course and risk factors for mortality of adult inpatients with COVID-19 in Wuhan, China: A retrospective cohort study. Lancet *395*, 1054–1062.

Zhou, P., Yang, X.-L., Wang, X.-G., Hu, B., Zhang, L., Zhang, W., Si, H.-R., Zhu, Y., Li, B., Huang, C.-L., et al. (2020b). A pneumonia outbreak associated with a new coronavirus of probable bat origin. Nature *579*, 270–273.

Zhu, N., Zhang, D., Wang, W., Li, X., Yang, B., Song, J., Zhao, X., Huang, B., Shi, W., Lu, R., et al.; China Novel Coronavirus Investigating and Research Team (2020). A novel coronavirus from patients with pneumonia in China, 2019. N. Engl. J. Med. *382*, 727–733.

Zou, L., Ruan, F., Huang, M., Liang, L., Huang, H., Hong, Z., Yu, J., Kang, M., Song, Y., Xia, J., et al. (2020a). SARS-CoV-2 viral load in upper respiratory specimens of infected patients. N. Engl. J. Med. *382*, 1177–1179.

Zou, X., Chen, K., Zou, J., Han, P., Hao, J., and Han, Z. (2020b). Single-cell RNA-seq data analysis on the receptor ACE2 expression reveals the potential risk of different human organs vulnerable to 2019-nCoV infection. Front. Med. *14*, 185–192.

STAR★METHODS

KEY RESOURCES TABLE

REAGENT or RESOURCE	SOURCE	IDENTIFIER
Critical commercial assays		
QIAseq FX DNA Library Kit	QIAGEN	180473
Quick-RNA Viral 96 Kit	Zymo Research	R1041
QIAseq SARS-CoV-2 Primer Panel	QIAGEN	333895
NEB Next Ultra II Directional RNA Library kit	New England Biolabs	E7760S
Deposited Data		
Raw data	This Study	Sequence Read Archive- BioProject SRA: PRJNA745169 (https://www.ncbi.nlm.nih.gov)
Healthy Nasal Microbiome	http://journal.frontiersin.org/article/10.3389/fmicb.2017.02372/full	European Nucleotide Archive - study number ENA: PRJEB23057 (https://www.ebi.ac.uk/ena/browser)
Oligonucleotides		
16S rRNA gene 515F forward primer 5′-GTGYCAGCMGCCGCGGTAA-3′	https://doi.org/10.1111/1462-2920.13023	N/A
16S rRNA gene 806R reverse primer 5′-GGACTACNVGGGTWTCTAAT-3′	https://doi.org/10.3354/ame01753	N/A
SARS-CoV-2 nucleoprotein qPCR forward primer 5′-GGGGAACTTCTCC TGCTAGAAT-3′	https://www.who.int/docs/default-source/coronaviruse/whoinhouseassays.pdf	N/A
SARS-CoV-2 nucleoprotein qPCR reverse primer 5′-CAGACATTTTG CTCTCAAGCTG-3′	https://www.who.int/docs/default-source/coronaviruse/whoinhouseassays.pdf	N/A
SARS-CoV-2 nucleoprotein qPCR probe 5′-FAMTTGCTGCTGCTTG ACAGATT-BHQ1-3′	https://www.who.int/docs/default-source/coronaviruse/whoinhouseassays.pdf	N/A
Human RNaseP qPCR forward primer 5′-AGATTTGGACCTGCGAGCG-3′	https://www.who.int/docs/default-source/coronaviruse/whoinhouseassays.pdf	N/A
Human RNaseP qPCR reverse primer 5′-GAGCGGCTGTCTCCACAAGT-3′	https://www.who.int/docs/default-source/coronaviruse/whoinhouseassays.pdf	N/A
Human RNaseP qPCR probe 5′-FAM-TTCTGACCTGAAGGC TCTGCGCG–BHQ1-3′	https://www.who.int/docs/default-source/coronaviruse/whoinhouseassays.pdf	N/A
Software and algorithms		
Quantitative Insights Into Microbial Ecology 2 (QIIME2)(2019.10) Built in tools: Dada2, mafft, sklearn, FastTree 2	http://www.nature.com/articles/s41587-019-0209-9	https://qiime2.org
GraphPad Prism 8	GraphPad Software Inc	http://www.graphpad.com:443
Metascape	10.1038/s41467-019-09234-6	https://metascape.org/
R software (v4.0.2) R packages: vegan (v2.5-7), SystemPipeR (v1.26.3), edgeR (v3.34.0), ggplot2 (v3.3.3)	R Foundation	https://www.r-project.org
GitHub of commands used in data analysis	This Study	https://github.com/NickRhoades/COVID-19_nasal_microboime

RESOURCE AVAILABILITY

Lead contact

Further information and requests for resources and reagents should be directed to and will be fulfilled by the lead contact, Ilhem Messaoudi (imessaou@uci.com).

Materials availability

This study did not generate new unique reagents.

Data and code availability

16S rRNA gene amplicon, host transcriptional and viral genome sequencing data have been deposited at the NCBI Sequence Read Archive (SRA) and are publicly available as of the date of publication. Accession numbers are listed in the key resources table. This paper does not report original code. However, a GitHub has been generated for the analysis of all sequencing data in this manuscript and can be accessed here (https://github.com/NickRhoades/COVID-19_nasal_microboime). Any additional information required to reanalyze the data reported in this paper is available from the lead contact upon request.

EXPERIMENTAL MODEL AND SUBJECT DETAILS

Human subjects

In this study we utilized excess material from samples originally collected for diagnostic purposes that would have otherwise been discarded. These samples were de-identified prior to being used for research purposes. As such the UC Irvine IRB determined that the data included in this manuscript did not qualify as human subject research and did not require IRB approval. All samples for this study were collected at University of California Irvine Medical center. Nasal swabs were collected from 68 SARS-CoV-2 positive patients (CoV+), 45 SARS-CoV-2 negative healthcare workers (HCW), and 21 SARS-CoV-2 negative patients (CoV-). Samples from CoV+ were collected at hospital admission. Samples from HCW were collected from otherwise healthy individuals as part of regular asymptomatic screenings. Samples from CoV- were collected from otherwise healthy individuals for asymptomatic screening prior to elective outpatient procedures. A full breakdown of subjects age and gender identity can be found in Table S1. Samples were collected between August and November 2020.

METHOD DETAILS

Sample collection, extraction, and SARS-CoV-2 RNA quantification

RNA was extracted from remnant de-identified nasal swab samples collected in viral transport medium (VTM) using the Quick-RNA^{TM} Viral 96 Kit (Zymo, Cat#R1041). SARS-CoV-2 viral loads were determined using qPCR with primers specific to the nucleoprotein (N). A one-step reaction was prepared using 5ul of extracted RNA or standard, 500nM of forward (5′-GGGGAACTTCTCCTGCTAGAAT-3′) and reverse (5′-CAGACATTTTGCTCTCAAGCTG-3′) SARS-CoV-2-nucleocapsid primers, 125 nM of SARS2-nucleocapsid probe (5′-FAM-TTGCTGCTGCTTGACAGATT-BHQ1-3′), and TaqPath 1-Step RT-qPCR Master Mix (Applied Biosystems, Foster City, CA, USA). PCR cycler conditions were 2 min at 95 °C, 15 min at 50 °C, denaturation for 2 min at 95 °C followed by 45 cycles of 3 s at 95 °C and 30 s 60 °C on the StepOnePlus Real-Time PCR System (Applied Biosystems, Foster City, CA, USA). An additional qPCR reaction was run on each sample using a primer/probe set to detect the human RNase P gene (RP) to control for extraction and sample quality. Blank extraction served as negative controls, while RNA extracted from SARS-CoV-2 cultures was used as Positive Template Control. All qPCR reactions were run in duplicates. Positivity was determined as a cycle threshold (Ct) value $\leq$ 40 for the N gene. Samples with a coefficient of variance > 20% were flagged to be re-run (none of the samples used in this study met this criteria). Samples were classified as: High Ct value (< 40- > 34.6-; n = 23); Mid Ct value (32.9-25.0; n = 23); and Low Ct values (< 23.5-15.8; n = 22).

16S amplicon libraries construction and data analysis

DNA that co-eluted with extracted RNA was used as the template to amplify the hypervariable V4 region of the 16S rRNA gene using PCR primers (515F/806R with the forward primer containing a 12-bp barcode) in duplicate reactions containing: 12.5 ul GoTaq master mix, 9.5 ul nuclease-free H20, 1 ul template DNA, and 1 ul 10uM primer mix. Thermal cycling parameters were 94°C for 3 minutes; 35 cycles of 94°C for 45 s, 50°C for 1 minute, and 72°C for 1 minute and 30 s; followed by 72°C for 10 minutes. PCR products were purified using a MinElute 96 UF PCR Purification Kit (QIAGEN, Valencia, CA, USA). Libraries were sequenced (2 × 300 bases) using Illumina MiSeq. Additional control samples were concurrently sequenced including extraction negative control, PCR blank negative control, and a microbial community standard positive control.

Raw FASTQ 16S rRNA gene amplicon sequences were uploaded and processed using the QIIME 2 version 2019.10 (Bolyen et al., 2019) analysis pipeline as we have previously described (Rhoades et al., 2019). Briefly, sequences were demultiplexed and quality filtered using the DADA2 plugin for QIIME 2 (Callahan et al., 2016), which filters chimeric and low-quality sequences. The generated sequence variants were then aligned using MAFFT (Katoh and Standley, 2013), and a phylogenetic tree was constructed using FastTree 2 (Price et al., 2010). Taxonomy was assigned to sequence variants using q2-feature-classifier against the SILVA Database (release: 138) (Quast et al., 2013). After taxonomic classification all sequences not assigned to a known phyla were removed along with any sequence assigned to mitochondria or chloroplast. Any Amplicon Sequencing Variant (ASV) that was found in > 1% abundance in either the extraction or PCR negative control and > 1% average abundance in samples was also removed. These ASVs were primarily assigned to two taxa which were highly abundant in the extraction controls (*Thermoanaerobacterium saccharolyticum* and Myxococcales 0319-6G20). We also found that *Streptococcus* was shared between the extraction control and samples, but these

sequences were not shared at the ASV level and therefore included in the dataset (Figure S1A). Finally, we confirmed a lack of PCR or sequencing bias using duplicate community standard samples (Figure S1A).

After clean up taxonomy was reassigned to sequence variants using q2-feature-classifier against the expanded Human Oral Microbiome Database (eHOMD: release version 15.21) (Escapa et al., 2018). This curated and site-specific database was used to improve species-level resolution. To prevent sequencing depth bias, samples were rarified to 8,000 sequences per sample before α and β diversity analysis. QIIME 2 was also used to generate the following α diversity metrics: richness (as observed taxonomic units), Shannon evenness, and phylogenetic diversity. β diversity was determined in QIIME 2 using weighted and unweighted UniFrac distances (Lozupone et al., 2011).

To confirm that microbial DNA co-eluted in our was reflective of a typical nasal microbiome community, we compared our data to a previously published nasal microbiome dataset (De Boeck et al., 2017). This study as it sampled a large number of healthy subjects and used the same amplicon primer set as our current study. Nasal microbiome data from this study was downloaded from (BioProject: PRJEB23057), merged with our dataset and analyzed using the exact parameters described above. Due to low sequencing depth of some samples in BioProject: PRJEB23057 after applying our analysis parameters, this combined dataset was rarified to 3000 sequences per sample prior to calculating α and β diversity metrics. A full analysis pipeline including parameters used for all commands can be accessed at https://github.com/NickRhoades/COVID-19_nasal_microboime.

RNA-seq library preparation and analysis

Quantity and quality of RNA extracted from 8 nasal swabs of (4 CoV+ and 4 HCW chosen at random, Table S1) was determined using an Agilent 2100 BioAnalyzer. cDNA libraries were constructed using the NEB Next Ultra II Directional RNA Library kit (Thermo Fischer). Briefly, RNA was treated with RNaseH and DNase I after depletion of ribosomal rRNA. Adapters were ligated to cDNA products. The ~300 bp amplicons were PCR-amplified and indexed with a unique molecular identifier. cDNA libraries were assessed for quality and quantity on the BioAnalyzer prior to single-end sequencing (x100bp) using the Illumina NovaSeq platform.

Bioinformatic analysis was performed using the systemPipeR RNA-Seq workflow (Backman and Girke, 2016). RNA-Seq reads were demultiplexed, quality-filtered and trimmed for quality and adaptor removal using Trim Galore (average Phred Score cut-off = 30, minimum length of 50 basepairs). Tophat was used to align filtered reads to the reference genome *Homo sapiens* (GRCh38). The file was used for annotation. Raw expression values (gene-level read counts) were generated using the summarizeOverlaps function and normalized (read per kilobase of transcript per million mapped reads, rpkm) using the edgeR package.

SARS-CoV-2 genome library construction and analysis

Enrichment for vRNA was performed using the QIASeq SARS-CoV-2 Primer Panel V2 (QIAGEN) Panel V2) followed by library construction with the QIAGEN FX DNA library preparation kit. Samples were indexed, pooled and validated with 2100 Agilent BioAn. Prior to Illumina sequencing (2x100bp, 1 M reads).

Adapters and primers were removed from demultiplexed sequencing readings using TrimGalore and MaskPrimers.py (pRESTO). Merged reads were aligned to SARS-CoV-2 Wuhan isolate NC_045512.2 with BWA-mem software version 0.7.17. Genomes with greater than 90% coverage and 10X depth were retained for phylogenetic analysis with Nextstrain. Amino acid changes and clade assignments were identified using Nextclade. A set of comparator sequences representing the original Wuhan isolate (NC_045512.2), variants of concern (B.1.351, EPI_ISL_960123; P.1, EPI_ISL_833167; B.1.1.7, EPI_ISL_659057), isolates from January 2020 New York (EPI_ISL_1293138) and Washington (EPI_ISL_404895), and representative isolates from California January-November 2020 (EPI_ISL_406036, EPI_ISL_411954, EPI_ISL_429875, EPI_ISL_436642, EPI_ISL_444023, EPI_ISL_569672, EPI_ISL_548382, EPI_ISL_548612, EPI_ISL_582897, EPI_ISL_625601, EPI_ISL_753324) were used for phylogenetic analysis. All sequences from Orange County, California from January 2020 to December 2020 were also retrieved from GISAID.

QUANTIFICATION AND STATISTICAL ANALYSIS

PERMANOVAs were performed using the Vegan (Dixon, 2003) function ADONIS. 1-way, non-parametric Kruskal-Wallis ANOVA were implemented using PRISM (V8) to generate p values and utilizing the Dunns post hoc-test when the initial ANOVA was significant. The LEfSe algorithm was used to identify differentially abundant taxa and pathways between groups with a logarithmic Linear discriminant analysis (LDA) score cutoff of 2 (Segata et al., 2011). For host transcriptional data edgeR was used to determine differentially expressed genes (DEGs) meeting the following criteria: genes with median rpkm of ≥ 1, a false discovery rate (FDR) corrected p value ≤ 0.05 and a $\log_2$fold change ≥ 1 compared to CoV- samples. Functional enrichment of DEGs was performed using Metascape to identify relevant Gene Ontology (GO) biological process terms (Zhou et al., 2019). Heatmaps, bar graphs and volcano plots were generated using R package ggplot2.

Cell Reports, Volume *36*

Supplemental information

Acute SARS-CoV-2 infection is associated with an increased abundance of bacterial pathogens, including *Pseudomonas aeruginosa* in the nose

Nicholas S. Rhoades, Amanda N. Pinski, Alisha N. Monsibais, Allen Jankeel, Brianna M. Doratt, Isaac R. Cinco, Izabela Ibraim, and Ilhem Messaoudi

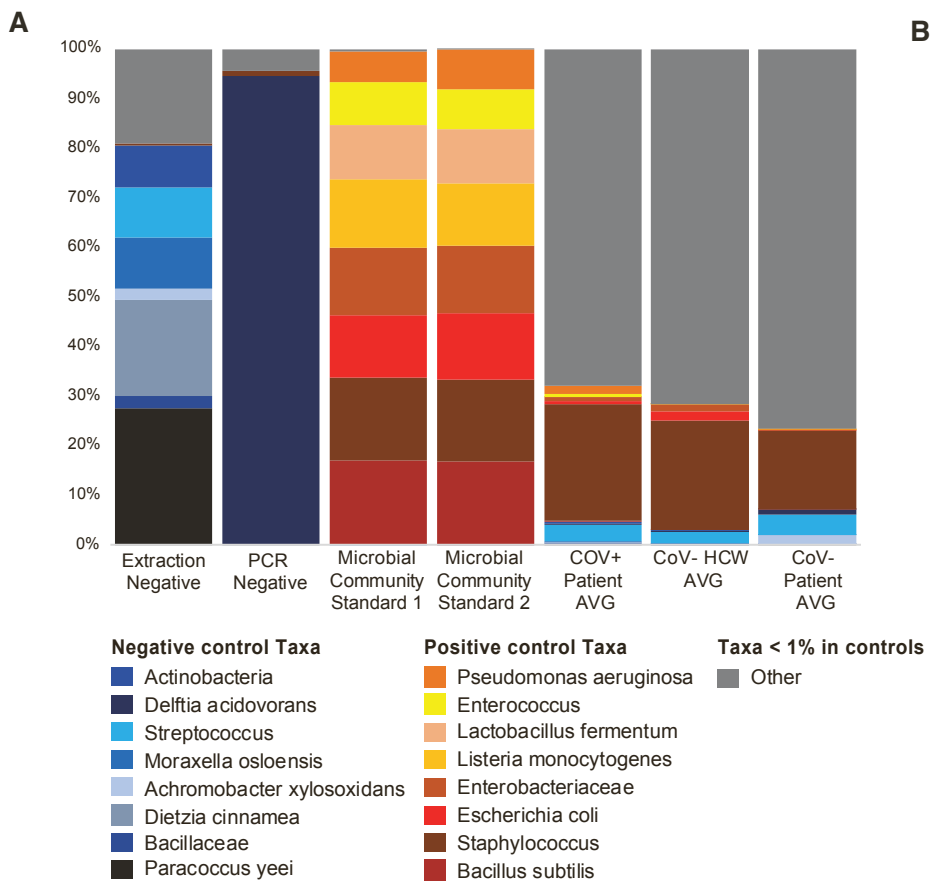

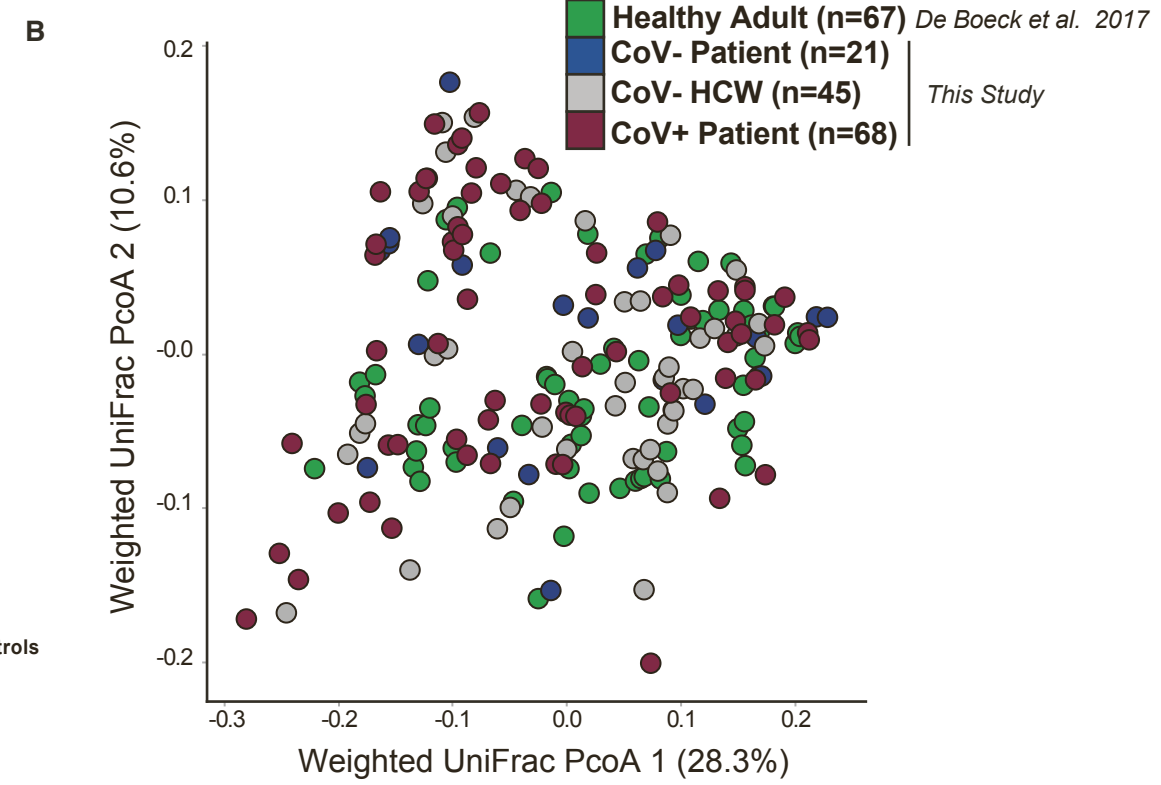

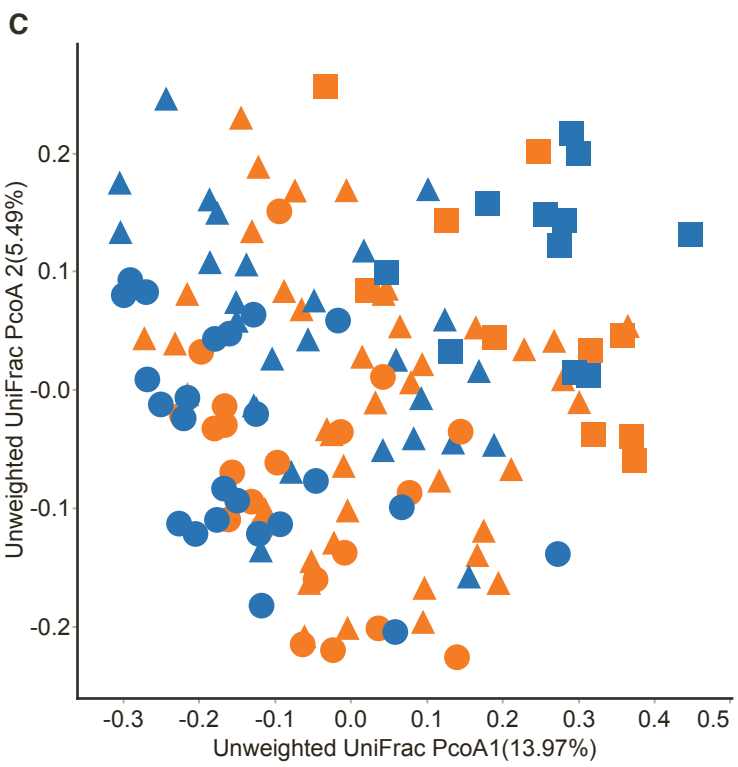

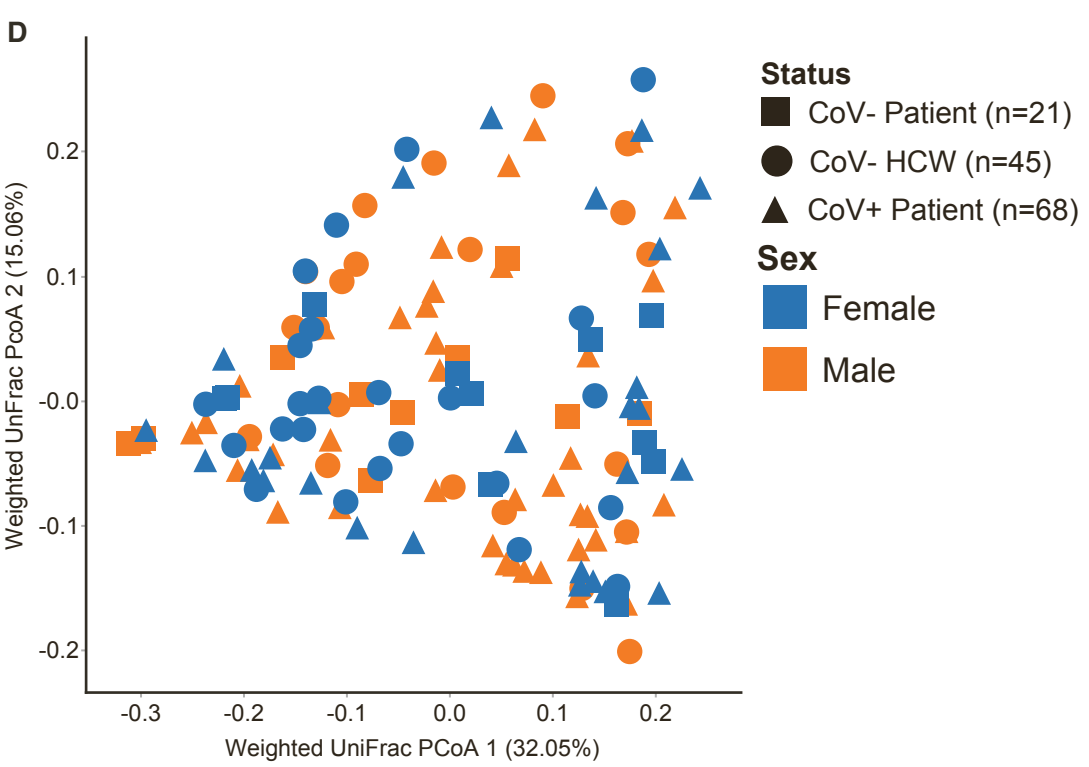

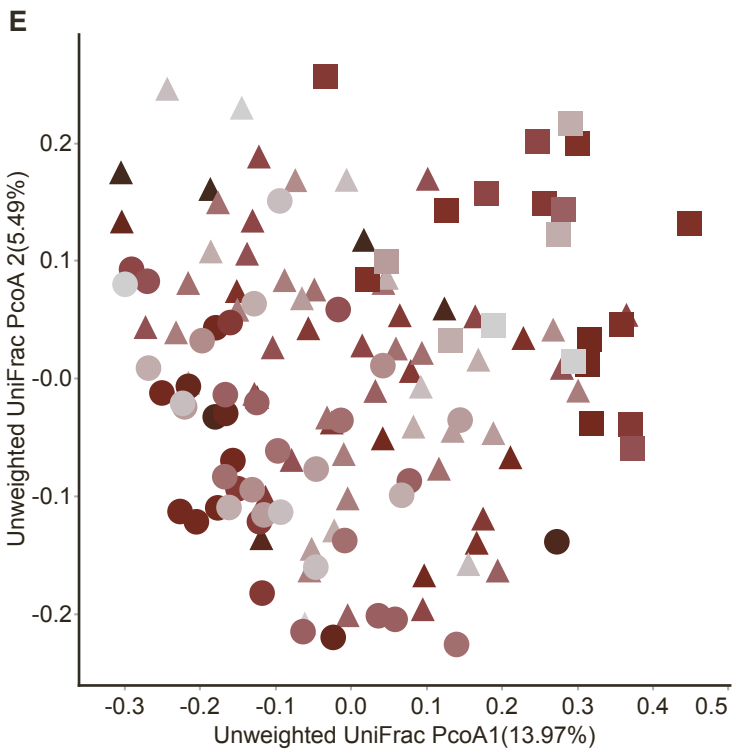

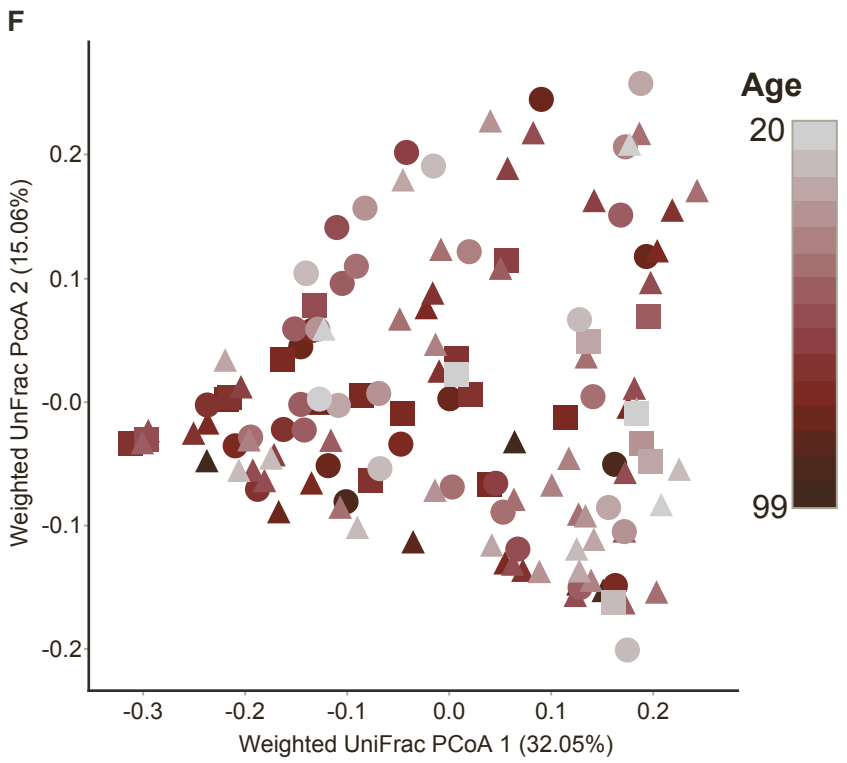

G

Unweighted UniFrac PERMANOVA	R^2	p
Status	**0.093**	**0.001**
Sex	**0.012**	**0.015**
Age	0.007	0.404
Sex within Status	0.014	0.279
Age within Status	0.012	0.78

H

Weighted UniFrac PERMANOVA	R^2	p
Status	**0.04**	**0.003**
Sex	0.006	0.506
Age	**0.016**	**0.033**
Sex within Status	0.014	0.428
Age within Status	0.016	0.318

Supplemental Fig. 1: DNA co-eluted following RNA exraction from viral transport medium is reflective of a nasal microbiome identified using conventional DNA extraction methods. Related to Figure 1. (A) Stacked bar plot highlighting taxa found in positive and negative control samples after removal of potential contaminating sequences, overlap of streptococcus between the extraction control and patient samples was not shared at the ASV level. (B) Principal-coordinate analysis of nasal microbiome weighted UniFrac distance including samples from this study and previously published "healthy" nasal microbiome data. (C-F) Principal-coordinate analysis of nasal microbiome unweighted (C,E) and weighted (D,F) distance including data only from this study colored by sex (C,D) and age (E,F). (G,H) The contribution of age, sex, age within status and sex within status to the total variance in the unweighted (G) and unweighted (H) UniFrac distance measured using PERMANOVA (Adonis with 999 permutations).

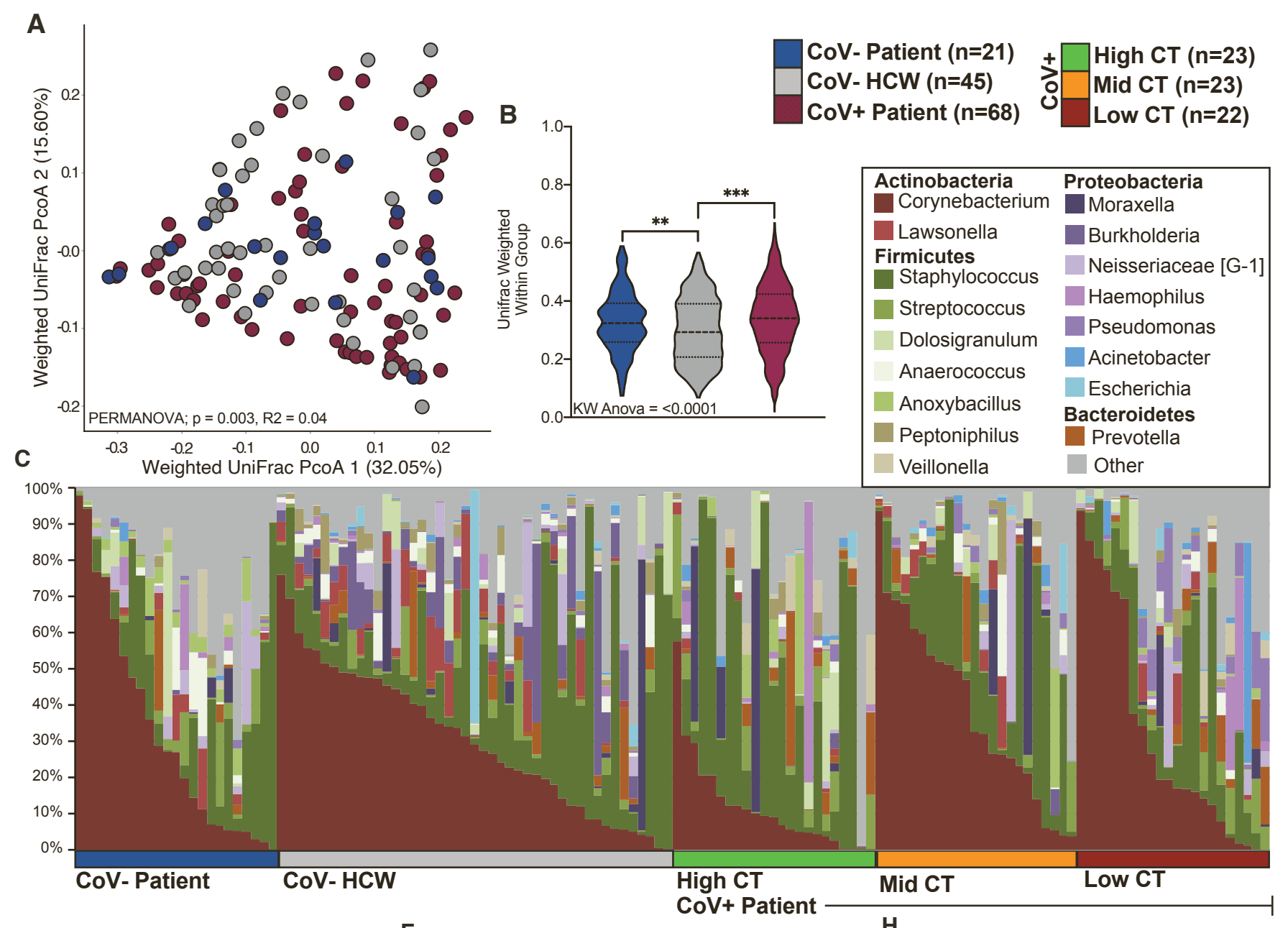

Supplemental Fig. 2: Additional features of the nasal microbiome associated with SARS-CoV-2 infection. Related to Figure 2. (A) Principal-coordinate analysis of nasal microbiome weighted UniFrac distance colored by host status. The contribution of host status to the total variance in the weighted UniFrac dissimilarity matrices was measured using PERMANOVA (Adonis with 10,000 permutations). (B) Violin plot illustrating average weighted UniFrac distances within each group. (C) Stacked bar of bacterial genera found at greater than 1% average abundance across the entire study population. Each vertical bar represents an individual sample and are ordered horizontally by host status. (D) Violin plot of Ct values generated via reverse transcription quantitative PCR of the SARS-CoV-2 Spike gene showing the distribution of samples within each CT group. (E) Violin plot of observed amplicon sequencing variants split by host Ct group within CoV+ patients. (F) Principal-coordinate analysis of nasal microbiome unweighted UniFrac distance colored by Ct group. The contribution of Ct value to the total variance in the weighted UniFrac dissimilarity matrices was measured using PERMANOVA (Adonis with 10,000 permutations). (G) Violin plot illustrating average unweighted UniFrac distances within each group. (H) Principal-coordinate analysis of nasal microbiome weighted UniFrac distance colored by Ct group. The contribution of the Ct to the total variance in the weighted UniFrac dissimilarity matrices was measured using PERMANOVA (Adonis with 10,000 permutations). (I) Violin plot illustrating average weighted UniFrac distances between each CT group. Significance for panels B,E,G,I was determined using Kruskal Wallis non-parametric ANOVA, with Dunn's multiple comparison * = $p < 0.05$, ** = $p < 0.01$, *** = $p < 0.001$, **** = $p < 0.0001$.

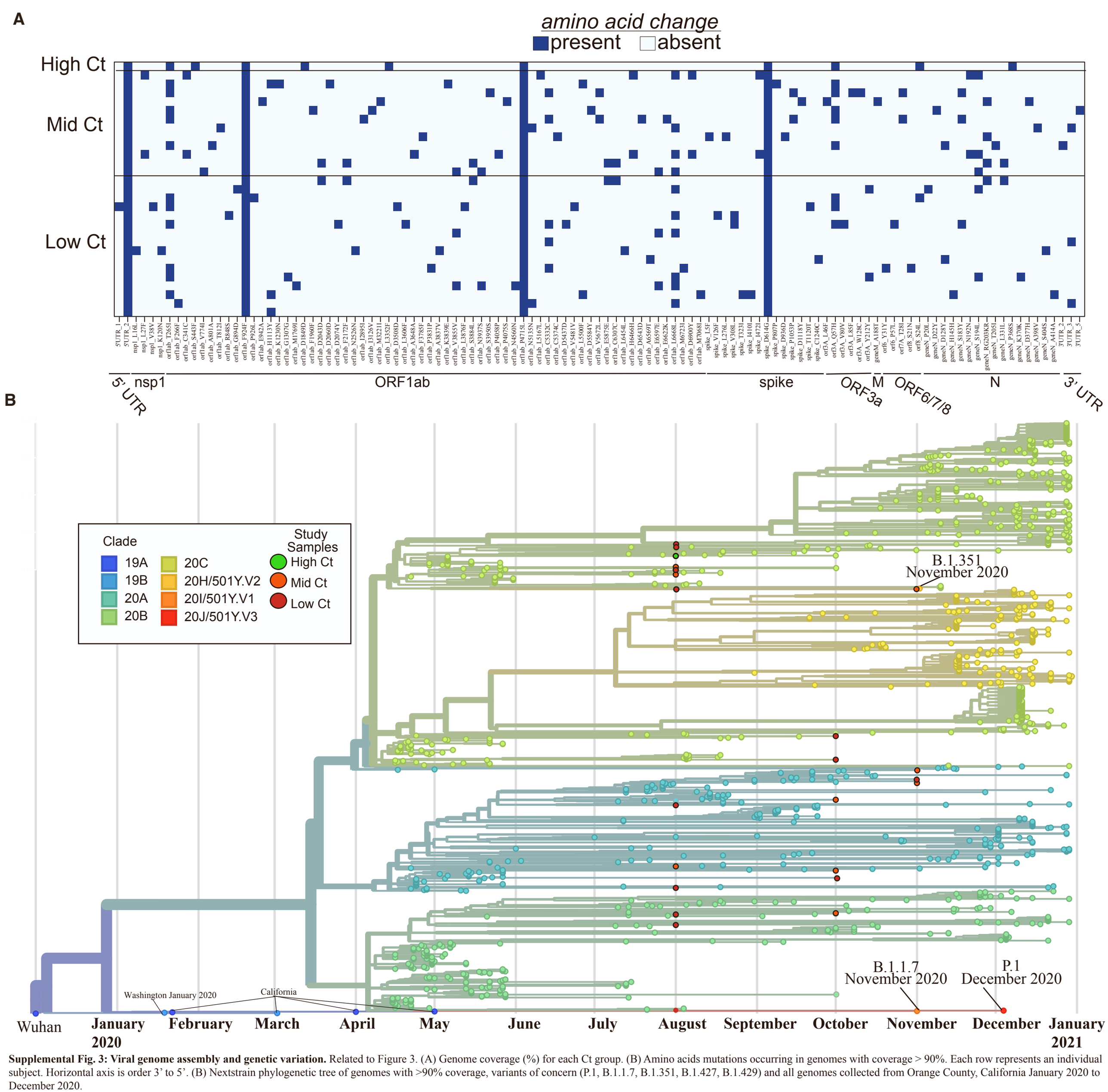

Supplemental Fig. 3: Viral genome assembly and genetic variation. Related to Figure 3. (A) Genome coverage (%) for each Ct group. (B) Amino acids mutations occurring in genomes with coverage > 90%. Each row represents an individual subject. Horizontal axis is order 3' to 5'. (B) Nextstrain phylogenetic tree of genomes with >90% coverage, variants of concern (P.1, B.1.1.7, B.1.351, B.1.427, B.1.429) and all genomes collected from Orange County, California January 2020 to December 2020.

Supplmental Table 1: Sample Metadata, Related to Figure 1. NA = Not Applicable.

SampleID	Status	CT_Value	CT_CAT	Age	Sex	Viral Genome	RNAseq	Microbiome
HCW_1	CoV- HCW	NA	NA	78	F	NA	No	Yes
HCW_2	CoV- HCW	NA	NA	55	F	NA	No	Yes
HCW_3	CoV- HCW	NA	NA	77	F	NA	No	Yes
HCW_4	CoV- HCW	NA	NA	76	F	NA	No	Yes
HCW_5	CoV- HCW	NA	NA	82	M	NA	No	Yes
HCW_6	CoV- HCW	NA	NA	55	M	NA	No	Yes
HCW_7	CoV- HCW	NA	NA	37	M	NA	No	Yes
HCW_8	CoV- HCW	NA	NA	55	M	NA	No	Yes
HCW_9	CoV- HCW	NA	NA	29	M	NA	No	Yes
HCW_10	CoV- HCW	NA	NA	80	M	NA	Yes	Yes
HCW_11	CoV- HCW	NA	NA	76	F	NA	No	Yes
HCW_12	CoV- HCW	NA	NA	83	M	NA	No	Yes
HCW_13	CoV- HCW	NA	NA	71	F	NA	No	Yes
HCW_14	CoV- HCW	NA	NA	91	M	NA	No	Yes
HCW_15	CoV- HCW	NA	NA	55	M	NA	No	Yes
HCW_16	CoV- HCW	NA	NA	48	M	NA	No	Yes
HCW_17	CoV- HCW	NA	NA	76	F	NA	No	Yes
HCW_18	CoV- HCW	NA	NA	28	M	NA	No	Yes
HCW_19	CoV- HCW	NA	NA	68	F	NA	No	Yes
HCW_20	CoV- HCW	NA	NA	53	F	NA	No	Yes
HCW_21	CoV- HCW	NA	NA	55	M	NA	No	Yes
HCW_22	CoV- HCW	NA	NA	50	M	NA	No	Yes
HCW_23	CoV- HCW	NA	NA	49	F	NA	No	Yes
HCW_24	CoV- HCW	NA	NA	91	F	NA	No	Yes
HCW_25	CoV- HCW	NA	NA	39	M	NA	No	Yes
HCW_26	CoV- HCW	NA	NA	66	F	NA	No	Yes
HCW_27	CoV- HCW	NA	NA	24	F	NA	No	Yes
HCW_28	CoV- HCW	NA	NA	36	M	NA	No	Yes
HCW_29	CoV- HCW	NA	NA	32	M	NA	No	Yes
HCW_30	CoV- HCW	NA	NA	30	F	NA	No	Yes
HCW_31	CoV- HCW	NA	NA	48	M	NA	No	Yes
HCW_32	CoV- HCW	NA	NA	30	F	NA	No	Yes
HCW_33	CoV- HCW	NA	NA	37	F	NA	No	Yes
HCW_34	CoV- HCW	NA	NA	29	M	NA	No	Yes
HCW_35	CoV- HCW	NA	NA	61	F	NA	No	Yes
HCW_36	CoV- HCW	NA	NA	33	F	NA	No	Yes
HCW_37	CoV- HCW	NA	NA	26	F	NA	No	Yes
HCW_38	CoV- HCW	NA	NA	35	F	NA	Yes	Yes
HCW_39	CoV- HCW	NA	NA	43	M	NA	No	Yes
HCW_40	CoV- HCW	NA	NA	50	M	NA	Yes	Yes
HCW_41	CoV- HCW	NA	NA	68	F	NA	No	Yes
HCW_42	CoV- HCW	NA	NA	82	F	NA	No	Yes
HCW_43	CoV- HCW	NA	NA	61	F	NA	No	Yes
HCW_44	CoV- HCW	NA	NA	42	M	NA	Yes	Yes
HCW_45	CoV- HCW	NA	NA	67	F	NA	No	Yes
COV_2	CoV+	38.076218	Hi	99	F	< 90% genome coverage	No	Yes
COV_3	CoV+	36.700247	Hi	55	M	< 90% genome coverage	No	Yes
COV_8	CoV+	37.806442	Hi	51	M	< 90% genome coverage	No	Yes
COV_10	CoV+	37.121967	Hi	26	F	No Library generated	No	Yes
COV_16	CoV+	39.08479	Hi	32	F	< 90% genome coverage	No	Yes
COV_17	CoV+	37.37857	Hi	67	F	< 90% genome coverage	No	Yes
COV_19	CoV+	37.56185	Hi	59	F	< 90% genome coverage	No	Yes
COV_24	CoV+	37.584984	Hi	79	M	< 90% genome coverage	No	Yes
COV_42	CoV+	37.14862	Hi	69	M	Yes	No	Yes
COV_48	CoV+	37.538563	Hi	34	M	< 90% genome coverage	No	Yes
COV_49	CoV+	38.944378	Hi	70	M	< 90% genome coverage	No	Yes

COV_50	CoV+	38.812202	Hi	30	M	< 90% genome coverage	No	Yes
COV_51	CoV+	37.67764	Hi	62	M	< 90% genome coverage	No	Yes
COV_53	CoV+	39.622738	Hi	91	F	< 90% genome coverage	No	Yes
COV_54	CoV+	38.347515	Hi	40	M	< 90% genome coverage	No	Yes
COV_55	CoV+	37.016968	Hi	25	M	No Library generated	No	Yes
COV_56	CoV+	38.229053	Hi	77	M	No Library generated	No	Yes
COV_57	CoV+	37.764614	Hi	62	M	No Library generated	No	Yes
COV_59	CoV+	39.776764	Hi	24	M	< 90% genome coverage	No	Yes
COV_61	CoV+	37.07317	Hi	45	M	No Library generated	No	Yes
COV_62	CoV+	37.32942	Hi	59	F	< 90% genome coverage	No	Yes
COV_63	CoV+	34.675777	Hi	49	F	< 90% genome coverage	No	Yes
COV_67	CoV+	34.74406	Hi	45	F	< 90% genome coverage	No	Yes
COV_1	CoV+	20.173272	Low	61	F	Yes	No	Yes
COV_5	CoV+	20.293746	Low	24	M	Yes	No	Yes
COV_18	CoV+	22.005283	Low	59	F	< 90% genome coverage	No	Yes
COV_21	CoV+	17.307197	Low	98	F	Yes	No	Yes
COV_23	CoV+	20.507776	Low	58	M	Yes	No	Yes
COV_25	CoV+	21.307083	Low	71	M	Yes	No	Yes
COV_26	CoV+	21.88542	Low	44	M	Yes	No	Yes
COV_27	CoV+	21.656952	Low	49	F	Yes	No	Yes
COV_28	CoV+	15.81649	Low	59	M	< 90% genome coverage	Yes	Yes
COV_30	CoV+	17.344656	Low	56	M	Yes	Yes	Yes
COV_33	CoV+	21.483639	Low	47	M	Yes	No	Yes
COV_34	CoV+	21.459263	Low	87	F	Yes	No	Yes
COV_35	CoV+	17.365662	Low	34	F	Yes	No	Yes
COV_39	CoV+	20.509508	Low	46	M	Yes	No	Yes
COV_40	CoV+	18.368208	Low	32	F	< 90% genome coverage	No	Yes
COV_41	CoV+	23.435507	Low	60	F	Yes	No	Yes
COV_43	CoV+	17.242144	Low	62	M	Yes	Yes	Yes
COV_44	CoV+	16.328108	Low	49	F	Yes	No	Yes
COV_46	CoV+	19.594623	Low	95	F	Yes	No	Yes
COV_64	CoV+	21.307083	Low	71	M	No Library generated	No	Yes
COV_66	CoV+	17.60019	Low	47	M	< 90% genome coverage	No	Yes
COV_68	CoV+	21.933756	Low	76	F	< 90% genome coverage	No	Yes
COV_4	CoV+	31.215872	Mid	30	M	< 90% genome coverage	No	Yes
COV_6	CoV+	29.00934	Mid	83	F	Yes	No	Yes
COV_7	CoV+	29.424534	Mid	51	M	Yes	No	Yes
COV_9	CoV+	29.59582	Mid	26	F	Yes	No	Yes
COV_11	CoV+	31.63975	Mid	33	F	< 90% genome coverage	No	Yes
COV_12	CoV+	31.136995	Mid	28	F	Yes	No	Yes
COV_13	CoV+	31.890806	Mid	65	M	No Library generated	No	Yes
COV_14	CoV+	30.049786	Mid	75	F	< 90% genome coverage	No	Yes
COV_15	CoV+	32.22774	Mid	52	M	< 90% genome coverage	No	Yes
COV_20	CoV+	30.898294	Mid	46	M	Yes	Yes	Yes
COV_22	CoV+	32.890465	Mid	51	M	< 90% genome coverage	No	Yes
COV_29	CoV+	25.006283	Mid	38	M	Yes	No	Yes
COV_31	CoV+	29.639048	Mid	70	M	Yes	No	Yes
COV_32	CoV+	32.694588	Mid	66	M	< 90% genome coverage	No	Yes
COV_36	CoV+	29.281885	Mid	56	M	Yes	No	Yes
COV_37	CoV+	31.368456	Mid	73	M	Yes	No	Yes
COV_38	CoV+	32.829716	Mid	77	F	< 90% genome coverage	No	Yes
COV_45	CoV+	31.100018	Mid	50	M	< 90% genome coverage	No	Yes
COV_47	CoV+	30.700317	Mid	32	M	< 90% genome coverage	No	Yes
COV_52	CoV+	29.120705	Mid	65	M	Yes	No	Yes
COV_58	CoV+	31.564772	Mid	36	F	Yes	No	Yes
COV_60	CoV+	29.432646	Mid	75	M	Yes	No	Yes
COV_65	CoV+	27.339397	Mid	40	M	< 90% genome coverage	No	Yes
NonCoV_1	CoV- patient	NA	NA	32	F	NA	No	Yes

NonCoV_2	CoV- patient	NA	NA	30	F	NA	No	Yes
NonCoV_3	CoV- patient	NA	NA	75	F	NA	No	Yes
NonCoV_4	CoV- patient	NA	NA	77	M	NA	No	Yes
NonCoV_8	CoV- patient	NA	NA	73	M	NA	No	Yes
NonCoV_9	CoV- patient	NA	NA	71	M	NA	No	Yes
NonCoV_10	CoV- patient	NA	NA	77	M	NA	No	Yes
NonCoV_12	CoV- patient	NA	NA	72	F	NA	No	Yes
NonCoV_13	CoV- patient	NA	NA	20	M	NA	No	Yes
NonCoV_14	CoV- patient	NA	NA	24	F	NA	No	Yes
NonCoV_16	CoV- patient	NA	NA	33	F	NA	No	Yes
NonCoV_17	CoV- patient	NA	NA	62	F	NA	No	Yes
NonCoV_18	CoV- patient	NA	NA	72	M	NA	No	Yes
NonCoV_19	CoV- patient	NA	NA	59	M	NA	No	Yes
NonCoV_20	CoV- patient	NA	NA	36	F	NA	No	Yes
NonCoV_22	CoV- patient	NA	NA	77	F	NA	No	Yes
NonCoV_23	CoV- patient	NA	NA	70	F	NA	No	Yes
NonCoV_24	CoV- patient	NA	NA	68	M	NA	No	Yes
NonCoV_26	CoV- patient	NA	NA	65	M	NA	No	Yes
NonCoV_27	CoV- patient	NA	NA	56	F	NA	No	Yes
NonCoV_28	CoV- patient	NA	NA	73	M	NA	No	Yes

Supplmental Table 2: Full LEFsE results, Related to Figure 2

Taxa	Group	Log10 LDA score	FDR p-value
g__Ochrobactrum	CoV+	2.811758395	0.0367078
g__Jeotgalicoccus	CoV+	3.076247372	0.0078099
g__Schaalia	CoV+	3.483370495	0.0175861
f__Bacillaceae___	CoV+	3.030009565	0.0343436
g__Dermabacter	CoV+	3.064796147	0.0036059
g__Micrococcus	CoV+	3.391801863	0.006672
g__Fastidiosipila	CoV+	3.070355684	0.0298342
g__Paracoccus	CoV+	2.916667243	0.0249822
g__Peptoniphilaceae__G_3_	CoV+	3.30527293	0.0098114
g__Fusobacterium	CoV+	3.289965814	0.002674
g__Pseudomonas	CoV+	4.001548907	0.0087463
g__Prevotella	CoV+	3.991703718	0.0225291
g__Moraxella	CoV+	4.211959633	0.0142522
g__Acinetobacter	CoV+	3.834024999	0.0110778
f__Enterobacteriaceae___	CoV+	3.035617222	0.0010228
g__Rothia	CoV+	3.044886859	0.0019198
g__Porphyromonas	CoV+	3.290269729	0.0162161
g__Brevundimonas	CoV+	2.825426652	0.0311487
g__Peptoniphilus	HCW	3.991241674	0.0002256
g__Capnocytophaga	HCW	2.997119911	0.0380345
g__Mycobacterium	HCW	3.362911231	0.0008491
g__Cardiobacterium	HCW	3.661581553	0.0243386
g__Klebsiella	HCW	3.744210715	0.0427925
c__Gammaproteobacteria_____	HCW	3.197456319	1.84E-09
g__Acidovorax	HCW	3.028770995	0.0241977
g__Finegoldia	HCW	3.515115664	0.0012149
g__Lawsonella	HCW	4.228442269	0.0001613
g__Lactococcus	HCW	3.675104466	0.0002873
g__Sphingomonas	HCW	3.437903649	0.0089651
c__Alphaproteobacteria_____	HCW	3.115002019	6.26E-06
g__Turicella	HCW	3.584602911	0.0003532
g__Burkholderia	HCW	4.546294251	7.17E-16
g__Escherichia	HCW	3.993386794	0.0196662
g__Cutibacterium	HCW	3.504843758	5.48E-15
g__Kocuria	HCW	3.143013983	0.0051622
g__Delftia	CoV-	3.692288734	0.0278583
g__Paenibacillus	CoV-	4.335964038	2.12E-19
g__Brevibacterium	CoV-	3.087982656	0.0394132
g__Anaerococcus	CoV-	3.995463034	0.0123125
g__Anoxybacillus	CoV-	4.223854276	9.19E-12
c__Betaproteobacteria_____	CoV-	4.065762597	8.34E-18